Open access • Journal Article • DOI:10.1063/1.5026973

A 4 K FT-ICR cell for infrared ion spectroscopy. — Source link

Lukas Fritsche, Andreas Bach, Larisa Miloglyadova, Alexandra Tsybizova ...+1 more authors

Institutions: ETH Zurich

Published on: 25 Jun 2018 - Review of Scientific Instruments (AIP Publishing LLCAIP Publishing)

Topics: Ion trap, Ion cyclotron resonance, Ion, Buffer gas and Spectroscopy

A 4 K FT-ICR cell for infrared ion spectroscopy

A 4 Kelvin FT-ICR Cell for Infrared Ion Spectroscopy

Lukas Fritsche, Andreas Bach, Larisa Miloglyadova, Alexandra Tsybizova and Peter Chen
Laboratorium für Organische Chemie, ETH Zurich, Vladimir-Prelog-Weg 2, CH-8093 Zürich, Switzerland

We present the design of the newly constructed cryogenic FT-ICR ion trap for infrared ion spectroscopy. Trapped ions are collisionally cooled by the pulsed introduction of buffer gas into the cell. Using different buffer gases and cell temperatures, we record action spectra of weakly bound neutral gas-analyte complexes using an IR laser source. We show for the first time that ion-He complexes can be observed in an ICR cell at temperatures around 4 K. We compare the experimental vibrational spectra of $Ag(PPh_3)_2^+$ obtained by tagging with different neutral gases: He, Ne, Ar, H_2 and N_2 to computed vibrational spectra. Furthermore, the conditions necessary for the formation of neutral tags within an ICR ion trap are studied.

I. INTRODUCTION

Vibrational spectroscopy reveals structural information of isolated ions in the gas phase, which brings additional dimension to gas phase experiments [1-10]. This is very important for mechanistic studies, and therefore different ion spectroscopy methods have been pushed forwards dramatically during the last decade.

Infrared action spectroscopy advanced significantly by the introduction of so-called infrared photodissociation (IRPD) technique. An important condition for this technique to work is the formation of weakly bound ion-neutral complexes between the ion and the buffer gas at low temperatures in the ion trap. The neutral molecules of the buffer gas are often referred to as "neutral tags" or "messenger species". The absorption of a single IR photon and subsequent redistribution of energy causes cleavage of the weak bond between the analyte and the neutral tag. Therefore, relatively low laser powers are used in IRPD experiments, which prevents power broadening of the absorption bands. Another advantage of the low ambient temperature is the lower number of populated rotational states and thus narrower band envelopes in the obtained vibrational spectra.

Current state-of-the-art mass spectrometry allows characterizing as well as effective storing and cooling of the ions to achieve high resolution [11-13]. Even though a growing number of research groups are able to spectroscopically probe reactive intermediates in the gas phase, those experiments remain challenging [14-19].

It is known that especially for small compounds, the nature of the messenger species does influence the vibrational frequencies of the analyte [18, 20]. Since we are interested in exploring transition metal complexes that are formed as intermediates in organometallic reactions, it is important to explore the influence of the messenger species by using different collision gases.

After Dopfer *et al.* pioneered the technique of tagging experiments with He [21-24], the observation of He-tagged ions in multipole ion traps has been reported.[15, 20, 25-27]. These rf traps must be followed by a separate ion detection system such as a time of flight (TOF) mass spectrometer, which necessarily means that the cell is emptied and refilled at each wavelength point in an IRPD experiment. On the other hand, Fourier-transform ion cyclotron resonance (FT ICR) ion traps can be used as mass analyzers themselves [28, 29]. ICR cells enable mass selection, analysis, ion storage and manipulation. The group of Niedner-Schatteburg has taken this approach before [19, 30, 31], but the temperature of their ion trap is not sufficiently low for tagging experiments with He, and, so far, no spectra using rare gases as tags in an ICR cell have been published.

In this work, we present the design and performance of a home-built cryo-FT-ICR cell designed for ion spectroscopy. The ICR cell can be cooled to temperatures below 4 K, and the pulsed supply of different buffer gases enables us to observe and probe different kinds of ion-neutral gas complexes within the cell. We validated the performance of our instrument by comparing measured vibrational spectra to those that have already published by other groups. To describe the conditions necessary to observe ion-neutral complexes in our ICR ion trap, we chose the $Ag(PPh_3)_2^+$ ion as a model complex. We present action vibrational spectra of $Ag(PPh_3)_2^+$ obtained by IRPD using different neutral tags: N_2, H_2, Ar, Ne and He. In addition, we evaluated the innocence of the different messenger species, especially with regard to instrumental conditions needed to obtain IR spectra with each tag. Lastly, we compared the experimental spectra to the calculated ones.

II. DESIGN

Figure 1 gives an overview of our FT-ICR mass spectrometer. The instrument consists of an electrospray ion source, a set of rf octopole ion guides, a quadrupole mass filter, a quadrupole ion bender, and the ICR cell that is connected to a two-stage, closed-cycle cryocooler. The ion optics as well as the cold instrument parts are located in a vacuum chamber that is separated into several differential pumping stages. The next sections describe the instrument in more detail.

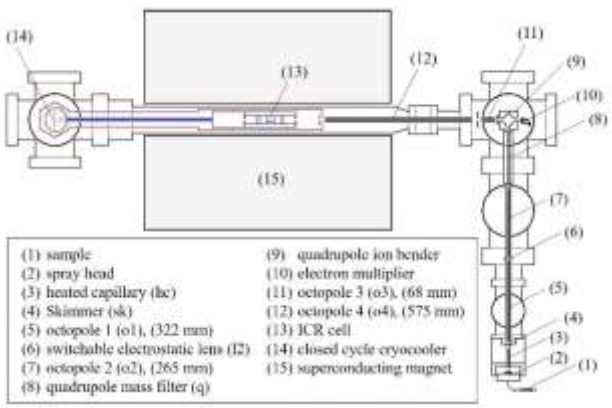

FIG. 1: Layout of the instrumental setup. Components connected to the cold part of the cryocooler are shown in blue. The outer radiation shields shown in red are connected to the warm stage of the cryocooler.

A. Ion Source

The ion source is a slightly modified electrospray source originally mounted on a Finnigan TSQ 700 instrument. The sample flows to the spray needle tip, which is held at a constant dc offset of 3–5 kV. The electrosprayed ions are transferred into vacuum through a heated capillary (Figure 1 (3)) with 0.5 mm inner diameter (ID) and 10 mm outer diameter. The capillary can be heated up to 250 °C. During the experiment, the heated capillary is usually held at around 170 °C and set to 50–120 V. A tube lens usually set to 35 V is located behind the heated capillary, followed by a skimmer cone electrode (1 mm ID), normally set to ground potential. The skimmer cone (Figure 1 (4)) separates the spray source chamber from the regions at higher vacuum.

B. Ion Guides

Ions generated by the spray source are guided by a set of four home-built rf octopole ion guides. The position of each rf ion guide is shown in Figure 1. Each octopole ion guide is made of eight 3 mm thick stainless steel rods arranged to form a cavity with an 8.5 mm diameter. The rods are held in place by a set of PEEK rod holders. On top of those, thin stainless steel disks with laser welded electrical contacts to the octopole rods are mounted. Figure 2 shows the design of an octopole ion guide used in our instrument. Other octopole ion guides vary in length and the number of PEEK holders. Each set of four non-neighboring rods is driven by a 1.5 MHz rf signal and the two rf signals are phase shifted by 180° from each other. The rf amplitudes are typically set to 200–300 V and the dc offset of the octopoles usually is between -2 and -30 V.

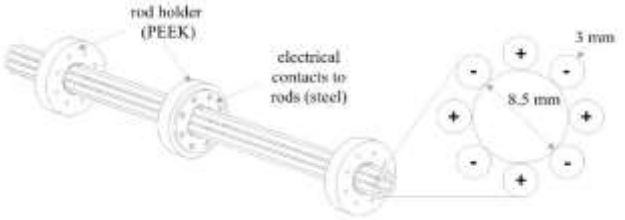

FIG. 2: General arrangement of the transfer octopoles used in the instrumental setup. Lengths of the octopoles differ according to their position within vacuum vessel.

The ions are accelerated by electrostatic lenses with 6–9 mm inner bore diameters that are placed in between the octopoles as well as after the octopole 2 and in front of the octopole 3. Figure 3 shows the arrangement and typical dc offset levels of the electrostatic components in front of the quadrupole ion bender.

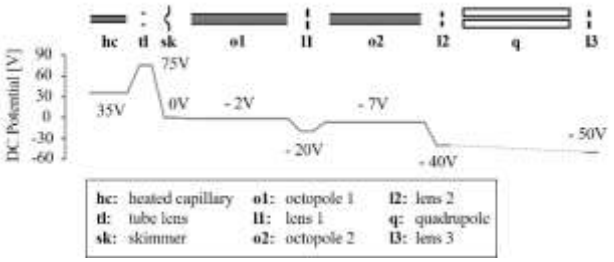

FIG. 3: dc levels on electrodes along the ion trajectory. The quadrupole dc level is not assigned because it depends on its mass resolution settings.

Octopole 1 can be used either as an ion guide or a trap. The operation mode is switched by applying either a high or a low potential offset at lens 1. When the dc potential is set to 20 V, the ions are stored during one duty cycle of one second. Switching the dc potential to -20 V for a few milliseconds, releases a packet of stored ions.

A good transmission of ions into the ICR cell is provided by setting the dc potential offsets on all components located in between the ICR cell (Figure 1 (13)) and the quadrupole ion bender (Figure 1 (9)) to -30 V.

C. Quadrupole Mass Filter and Ion Bender

The quadrupole mass filter (Extrel CMS, LLC, Pittsburgh, PA) allows for transmission of ions in the range of *m/z* 2–2000. After mass selection, the ions are deflected by a quadrupole ion deflector (Extrel CMS). For this purpose, the electrostatic potential on two orthogonal pairs of opposing rods is set to -45 V and -400 V respectively. To reverse the deflection angle these potentials can be switched. The ions are either guided towards the ICR cell or are detected by an electron multiplier (Extrel CMS, see Figure 1 (10)) which includes a conversion dynode. This detector is used to analyze the sprayed solution and to estimate roughly the number of ions being transferred towards the ICR cell. To obtain a better trapping efficiency in the ICR cell, the quadrupole mass filter is set to the single ion-monitoring mode and the resolution is usually decreased for a better ion throughput.

D. Cryo-FT-ICR Cell

Figure 4 shows a three-quarter cut model of the FT-ICR cell used in our instrument. It consists of seven segments along the cylinder axis, all made of gold-coated copper. The inner diameter of the cell is 28 mm and the segments are 3 mm thick. All segments are isolated by a 1 mm aluminum oxide ceramic spacer. A set of eight 1.5 mm diameter aluminum oxide ceramic rods aligns and supports the cell segments. Two gold-coated copper disks hold the segments together in the axial dimension. The copper disks are connected by four gold-coated copper rods. The ring electrode is further split into four segments. The detection plates each span an angle of 119° and the excitation plates each span an angle of 59° (Figure 4).

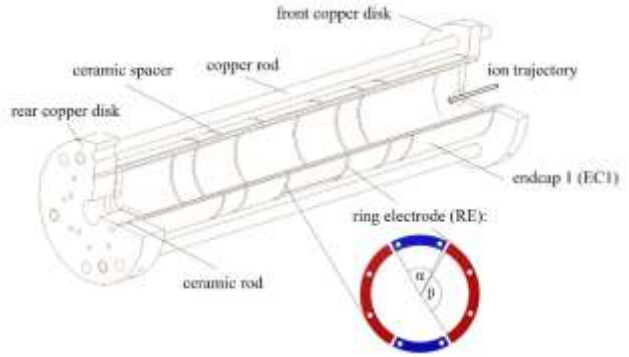

FIG. 4: The design of the cryo-FT-ICR cell. A cut through the ring electrode orthogonal to the axial direction is sketched at the bottom. The excitation electrodes (blue) span an angle of 59° each and the detection electrodes (red) span an angle of 119° each.

The relative dimensions of the electrode segments as well as the relative dc potentials have been adapted from the cell developed for ISOLTRAP at ISOLDE/CERN [32], except for the length of the endcap electrodes, which are somewhat shorter in our instrument (Table I). Typically, the endcap potentials are set to 0 V and the trapping potential is -5–-10 V.

TABLE I: lengths of the electrode segments of the ICR trap as well as the applied potentials in units of the potential difference between the ring electrode and the outer endcap electrodes.

electrode	l_i (mm)	V_i/V_0
endcap 1 (EC1)	44.5	0
correction electrode 1 (CE1)	11.6	0.34
correction electrode 2 (CE2)	22.2	0.83
ring electrode (RE)	32.3	1.00
correction electrode 3 (CE3)	22.2	0.83
correction electrode 4 (CE4)	11.6	0.34
endcap 2 (EC2)	44.5	0

Voltages on both endcaps can be switched rapidly, creating two different cell arrangements: open and closed (Figure 5). In the open cell arrangement, ions enter the cell and are deflected at the opposite endcap. Collisions with a buffer gas reduce the kinetic energy of the ions, such that the symmetrical potential well used in the closed cell arrangement cannot be surmounted.

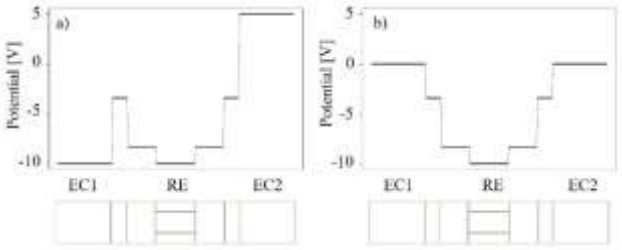

FIG. 5: Shapes of the potential well formed by the application of different dc potentials to the ICR cell segments at a 10 V trapping potential. (a) Open cell arrangement. Cations coming from the left side pass the lowered EC1 potential and are stopped by the higher potential of EC2. (b) Closed cell arrangement with symmetrical potential well.

The ICR cell is centered within the homogeneous field regime of a 4.7 T superconducting magnet (Cryomagnetics, inc., Oak Ridge, TN) with a diameter of the horizontal bore of 127 mm. A stainless steel tube with a 100 mm inner diameter, reaching through the whole magnet bore, separates the high-vacuum region surrounding the ICR cell from the atmosphere.

A gold plated copper rod (614 mm long, 20 mm in diameter) thermally connects the ICR cell with the cold stage of a closed-cycle pulse tube cryocooler (Cryomech, Inc., PT415-RM, Syracuse, NY, Figure 1 (15)). Two radiation shields surround the cell. The inner shield is directly wrapped around the copper disks that hold and stabilize the cell thus being connected to the cold stage of the cryocooler as well. The outer shield is only connected to the warm stage of the cryocooler to prevent the cell from the blackbody radiation heating. All radiation shields are made of gold-coated copper. The temperature inside the instrument is measured at four places using silicon diodes (Lakeshore Cryotronics, Inc., Westerville, OH). Two of the diodes are placed directly at the warm and the cold stage of the cryocooler, one at the ICR cell and one at the outer radiation shield. This setup allows reaching less than 4 K at the ICR cell during experiments. In addition, to vary the cell temperature, a 100 W cartridge heater (Lakeshore Cryotronics, Inc., HTR-25-100) is attached to the warm stage, and a 50 W cartridge heater (Lakeshore Cryotronics, Inc., HTR-50) is attached to the cold stage of the cryocooler. The temperature can be actively controlled and monitored by a cryogenic temperature controller (Lakeshore Cryotronics, Inc., Model 336). The setup can be cooled from room temperature to 4 K in less than 5 h (see SI).

The buffer gas is introduced through a pulsed valve (General Valve, corp., Series 9, Pine Brook, NJ) mounted on a flange close to the warm stage of the cryocooler. It then flows through a stainless-steel tube (with 1/8 inch inner diameter and a total length of ca. 1.5 m) that connects the valve with the ICR cell. The steel tube is in thermal contact to both, warm and cold stage of the cryocooler, such that the buffer gas is pre-cooled in the tube before admission to the cell.

E. Vacuum System

The vacuum chamber is divided into several differentially pumped stages. In the source chamber, where

the heated capillary and the tube lens are located, a 27 m^3/h multi-stage roots pump (Pfeiffer Vacuum GMBH, ACP 28, Asslar, DE) maintains a pressure of 6×10^{-2} mbar. A Pirani gauge (Pfeiffer Vacuum GMBH, TPR 280) monitors the pressure in this stage.

The pressure in the next stage, where octopole 1 (Figure 1 (5)) is located is 2.5×10^{-5} mbar. This pressure is maintained by a 260 l/s turbomolecular pump (Pfeiffer Vacuum GMBH, HiPace 300) and measured by a cold cathode gauge (Pfeiffer Vacuum GMBH, PKR 251). The ACP 28 multi-stage roots pump that is used to pump the source chamber also backs this turbomolecular pump.

A bigger 650 l/s turbomolecular pump (Pfeiffer Vacuum GMBH, HiPace 700) evacuates the octopole 2 (Figure 1 (7)) region. It is backed by a 14 m3/h multi-stage roots pump (Pfeiffer Vacuum GMBH, ACP 15).

The next 650 l/s turbomolecular pump (Pfeiffer Vacuum GMBH, HiPace 700) is attached to the quadrupole deflector (Figure 1 (9)) region and maintains the pressure of less than 5×10^{-9} mbar. This turbomolecular pump is backed by a shared connection to the afore mentioned ACP 15 pump.

The cryocooler region is pumped by another 650 l/s turbomolecular pump (Pfeiffer Vacuum GMBH, HiPace 700). A 14 m^3/h multi-stage roots pump (Pfeiffer Vacuum GMBH, ACP 15) backs this turbomolecular pump. The pressure in this stage is 3×10^{-8} mbar at room temperature. Without buffer gas, at 4 K, the pressure drops to 1.5×10^{-10} mbar due to cryopumping.

F. Electronics

A 16-channel high voltage (± 500 V_{DC}) power supply (Stahl Electronics, HV 500-16, Mettenheim, DE) provides the voltage for electrostatic elements such as the heated capillary, the tube lens, electrostatic lenses, octopole dc levels and the quadrupole ion bender. The 16-channel high precision (± 15 V_{DC}) power supply (Stahl Electronics, BS 1-16) provides the voltage for all the ICR cell electrodes and for some of the lens and octopole dc offsets. Elements with variable dc offset levels such as the end cap electrodes of the ICR cell and lens 1 are connected to two-channel high voltage switches (Stahl Electronics, HS 200). Three high voltage power supplies (iseg Spezialelektronik GMBH, DPS Series, Radeberg, DE) provide the voltage for the spray needle, the conversion dynode and the electron multiplier.

Two homemade rf generators running at ca. 1.5 MHz each provide the rf voltage with a variable amplitude for two octopoles each. The 1.2 MHz-rf power supply for the quadrupole mass filter was purchased from Extrel.

A variable gain low noise current amplifier (FEMTO Messtechnik GMBH, DLPCA-200, Berlin, DE) amplifies the signal obtained at the electron multiplier after mass selection by the quadrupole mass filter. A low noise cryogenic amplifier (Stahl Electronics, XC-4 cryogenic amplifier) located in direct proximity to the ICR cell, preamplifies the signal picked up from the detection electrodes. A room temperature amplifier and biasing tool (Stahl Electronics, A3–5b), mounted on a flange outside the vacuum vessel further amplifies the signal and provides the biasing currents for the cryogenic preamplifier.

We use a National Instruments PXI Chassis that houses two 14-bit, 100 MS/s arbitrary waveform generator (AWG) cards, a 14-bit, 100 MS/s analog to digital converter (ADC) card and two R-series interface cards for field programmable gate arrays (FPGA). The AWGs apply the excitation rf signal to each of the excitation electrodes. The ADC digitizes the amplified differential signal picked up at the detection electrodes. Two FPGAs (National Instruments™) control the operation modes and triggering for the quadrupole mass filter and the FEMTO amplifier. LabVIEW programs were written for data evaluation and visualization and for the control of all electronics. An external delay generator (Stanford Research Systems, DG645, Sunnyvale, CA) serves as master clock for all timed processes and triggers the pulsed valve for the buffer gas inlet. Events of voltage switching and the master trigger for excitation and detection of trapped ions are controlled by a second delay generator (Stanford Research Systems, DG535). All other timed events are controlled by the PXI.

G. Laser setup

We produce laser light by two-stage difference frequency mixing of the output of a Nd:YAG laser (14.5 ns, f = 20 Hz, λ = 1064 nm) (Spectra Physics, Quanta Ray, GCR-200, Santa Clara, CA) and a tunable Dye Laser (Radiant Dyes Laser & Accessories GmbH, NarrowScan, Wermelskirchen, DE). A schematic setup is shown in Figure 6.

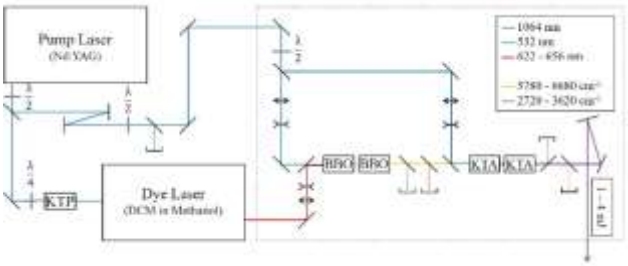

FIG. 6: Schematic overview of the setup for the generation of tunable infrared laser light. Difference frequency mixing is achieved in a set of two BBO and two KTA crystals.

A part of the output of the pulsed Nd:YAG laser is frequency doubled in a KTP crystal to 532 nm and used to pump the tunable, pulsed dye laser. For the experiments presented in this paper, only the oscillator of the Nd:YAG was used and no injection seeder was installed. Tunable laser light in the range of 622–659 nm was obtained by using DCM in methanol in the dye laser. The output of the pump- and the dye-laser were mixed in a set of two BBO crystals. The resulting idler wave was mixed again in a set of two KTA crystals with the output of the Nd:YAG laser. The resulting spectral range lies between 2700 and 3600 cm^{-1} with pulse energies between 1 and 4 mJ and a band width of approximately 1.2 cm^{-1}.

III. EXPERIMENTAL

A. Chemicals

All of the chemicals mentioned in this work were purchased from Sigma Aldrich and used without further purification. In most of the experiments, we used a 100 µM solution of silver nitrate and triphenylphosphine in methanol. When subjected to electrospray it produces a strong signal of bis(triphenylphosphine)silver(I) ($Ag(PPh_3)_2^+$) cation. This ion is observed at *m/z* 631 and shows a characteristic isotope pattern of a silver cation. Although it is an unreactive ion, it is otherwise similar in size and complexity to many of the complexes used in organometallic reactions and therefore represents a good model complex for our studies.

B. Mass spectrometric experiments

After pre-selection in the quadrupole mass filter, the ions are guided into the FT-ICR cell. A duty cycle time of 1 s was chosen. During one duty cycle, a gas pulse is released into the cell. Simultaneously, a packet of ions is transferred from octopole 1 by switching lens 1 to a lower potential. The ions are trapped by endcap switching, and, after a time delay for buffer gas cooling, excited before the image current is detected. Figure 7 shows a summary of the triggered events during one duty cycle, including the rough timings.

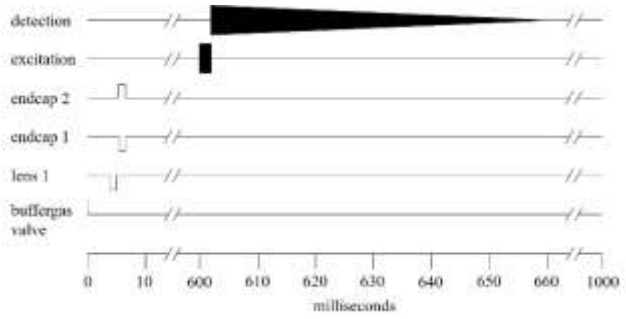

FIG. 7: Schematic timing of events during one duty cycle of the instrument. After trapping, the ions are stored and collisionally cooled by the buffer gas for ca. 600 ms.

The ions are stored and accumulated for several cycles inside the ICR trap. The time domain signal is collected and Fourier transformed after the application of a stored waveform inverse Fourier transform (SWIFT) [33, 34] excitation pulse with a duration of typically 2 ms. Efficient trapping and the formation of ion-neutral complexes can be achieved at a steady-state buffer gas background pressure in the order of 10^{-8} mbar. The effective pressure within the ion trap is estimated to be at least three orders of magnitude higher (see Supporting Information). The cell temperature is varied between 4 and 65 K depending on the buffer gas that is used for the experiment. At such high pressures, the magnetron motion of trapped ions can dramatically perturb the obtained mass spectra. To improve the quality of the mass spectra, one or several "axialization" pulses, implemented as two-plate azimuthal quadrupolar excitation [35, 36] of variable duration and amplitudes can be applied to reduce the magnetron radius.

C. Vibrational Spectroscopy

In the collision cell, we usually observe a steady state system composed of tagged and untagged ions. In the case of sustained light absorption the balance shifts, and a new steady state is established. Therefore, we irradiated the trapped ions at least for several seconds until the relative peak intensities of tagged and untagged ions do not change anymore. A diaphragm beam shutter (Thorlabs, Inc., SHB1T, Newton, NJ) blocked the beamline when necessary. For every given wavenumber we recorded relative peak intensities of tagged and untagged ions with the open and closed laser beamline. The relative changes in the signal were then evaluated as a function of the photon energy. The infrared region is scanned in a stop-collect-move laser type of protocol. The laser beam is not focused and fills the whole 6 mm entrance cavity of the ICR cell. Because the laser source is not synchronized with the excitation and detection of ions and because the cyclotron radius quickly relaxes due to the large background pressure, we assume a total overlap of the laser beam with the ion cloud if the magnetron radius is small.

D. DFT calculations

Density functional theory (DFT) calculations were performed with the Gaussian 09 package [37]. The combination of the BP86 method with two different basis sets was applied. For the geometry optimizations of the initial $Ag(PPh_3)_2^+$ complex as well as for the calculations of its harmonic vibrational spectra, def2-TZVP basis set was used. The def2-SVP basis set was employed for the optimization and frequency calculations of the tagged complexes, as well as for anharmonic VPT2 calculations [38, 39].

Frequency analysis enabled calculation of thermochemical correction and confirmed the optimized structures as local minima on the potential energy surfaces. All energies reported include zero point energies.

IV. RESULTS

A. Mass Spectra

Typical mass spectra of the $Ag(PPh_3)_2^+$ ion and its ion-neutral complexes with different messenger species are shown in Figure 8. The characteristic isotope pattern of $Ag(PPh_3)_2^+$ consists of four peaks: two main peaks at *m/z* 631 and 633 resulting from the two silver isotopes (^{107}Ag and ^{109}Ag) and the two peaks at *m/z* 632 and 634 resulting from the corresponding ^{13}C satellites. When N_2 is introduced as buffer gas into the cell at a temperature of ca. 48 K, several additional signals appear. All of them show the same characteristic isotope pattern, and the signals are separated by a mass difference of 28 amu. Under the conditions used for the mass spectrum in Figure 8 (b), our

model complex favors the attachment of two nitrogen molecules. On the other hand, when pure Ne is introduced as buffer gas, ion-neutral complexes with one and two neon atoms can be observed. The untagged ion peaks remain the most intense ones (Figure 8 (c)). For H_2, the most intense peak could be observed with seven hydrogen molecules attached at a cell temperature of 14 K. The number of attached messenger molecules and the corresponding peak intensities generally depend on the environmental conditions within the ICR cell. Furthermore, the excitation time and amplitude affect the relative peak intensities.

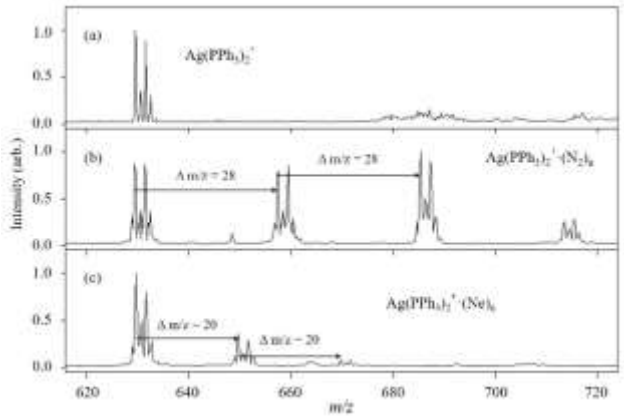

FIG. 8: Typical mass spectra of the $Ag(PPh_3)_2^+$ ion obtained with different buffer gases. (a) The $Ag(PPh_3)_2^+$ ion recorded with He as buffer gas but at slightly higher temperatures than those required for He-tagging. (b) N_2 is used as buffer gas at a cell temperature of 48 K. (c) Ne is used as buffer gas at a cell temperature of ca. 9 K.

The observation of ion-neutral complexes with noble gases is generally more difficult. Not surprisingly, the intensity of the ion neutral complexes relative to the untagged species usually drops as the polarizability of the messenger species decreases. For the $Ag(PPh_3)_2^+$ model complex, the cell temperatures at which ion-neutral complexes could be observed were ca. 42 K for argon, 9 K for neon and 4 K for helium. Figure 9 shows a mass spectrum taken under He-tagging conditions. In addition to the peaks corresponding to the pure $Ag(PPh_3)_2^+$ cation, weak signals corresponding to species tagged with one and two helium atoms appear.

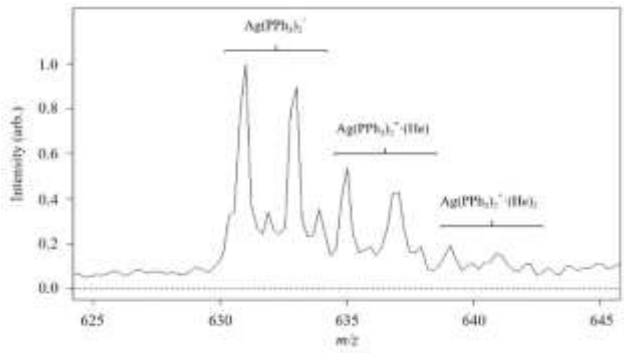

FIG. 9: Mass spectrum of the bis(triphenylphosphine)silver(I) cation with pure He as buffer gas at a cell temperature of 4 K and He background pressure of 2×10^{-8} mbar.

The formation of ion-neutral complexes strongly depends on the buffer gas pressure within the ion trap and the temperature of the ICR cell. Figure 10 shows the measured peak intensities of the untagged $Ag(PPh_3)_2^+$ ion and the corresponding complex bearing a single helium atom as a function of temperature and pressure.

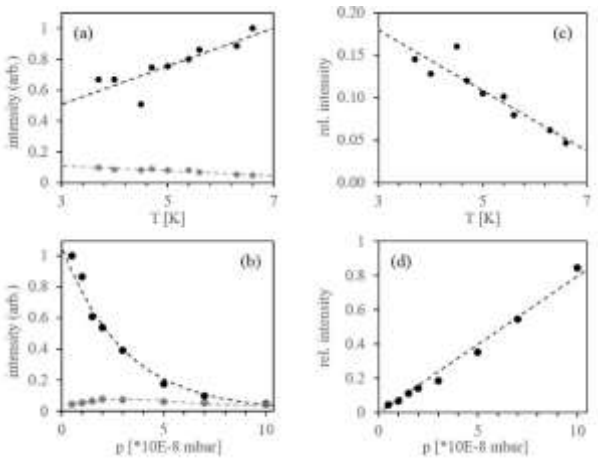

FIG. 10: Dependencies of the peak intensities for He-tagged signals on cell temperature and background pressure. The black dots on the diagrams (a) and (b) represent the absolute signal intensities of the first untagged species (*m/z* 631) whereas the gray dots represent the signal intensities of the species with a single tag (*m/z* 635). The pressure was kept at 3×10^{-8} mbar. The dots in diagrams (c) and (d) represent the relative signal intensities of the tagged *vs.* the untagged species. The cell temperature was 4 K.

Diagrams (a) and (c) in which the temperature was varied, were recorded at a background pressure of 3×10^{-8} mbar. For the diagrams (b) and (d) the temperature was held at 4 K. At higher cell temperatures, the fraction of He-tagged $Ag(PPh_3)_2^+$ decreases. No tagged complexes could be observed above 7 K. Therefore, a lower temperature is favorable for the formation of ion-He-complexes, as would be expected. Higher buffer gas background pressures lead to a larger relative intensity of the tagged *vs.* untagged species. However, the overall signal intensity exponentially decreases with an increasing background pressure. In this case, a background pressure of 3×10^{-8} mbar seems to be the most suitable for the recording of infrared spectra.

B. Vibrational Spectra

The presented instrument was constructed for the vibrational analysis of cold ions in the gas phase. The performance of the instrument in this respect was tested again on the $Ag(PPh_3)_2^+$ model complex in the range of 3000–3150 cm^{-1}. Here, the IR spectrum should show the aromatic C-H vibrations of the monosubstituted phenyls. Figure 11 shows the mass spectra of H_2-tagged $Ag(PPh_3)_2^+$ complexes with the open and closed laser beamline at a photon energy of 3078 cm^{-1}, where the model complex absorbs. Changes in the mass spectrum are observed if the photon energy matches the vibrational band of the complex ion. However, if the photon energy does not match a vibrational band, the mass spectra taken with open and closed beamline do not show significant differences.

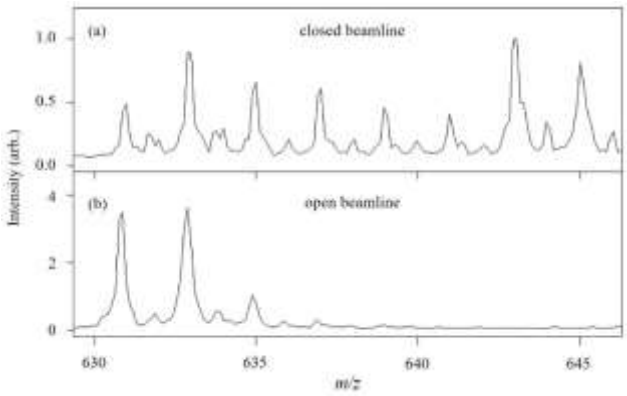

FIG. 11: Mass spectra of the H_2-tagged $Ag(PPh_3)_2^+$ with the (a) blocked beamline, (b) open beamline. The trapped ions are irradiated with a photon energy of 3078 cm^{-1}.

For every given wavenumber we determine the change in relative intensity of untagged and tagged peaks. This change is then compared to the change in relative peak intensity of the corresponding pair of ions when the beamline is closed. The resulting vibrational action spectra are shown in Figure 12.

When the photon energy matches a vibrational transition, not necessarily all of the neutral tags are cleaved off the ions. In general, we observe that the distribution of mass signals shifts to lower number of attached messenger molecules. If tagged species with more than one tag are observed, the sensitivity of absorption detection increases if species with a higher number of attached tags are selected for the data evaluation. However, to generate better vibrational spectra, we usually select peaks of the tagged species with the highest intensity.

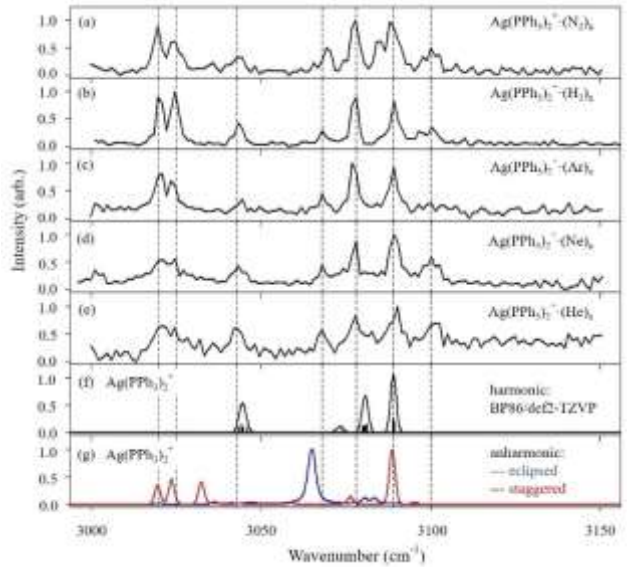

FIG. 12: Vibrational action spectra of the $Ag(PPh_3)_2^+$ model complex using different messenger species for neutral tagging experiments. The cell temperature and the neutral gas were (a) N_2 at ca. 48 K, (b) H_2 at ca. 14 K, (c) Ar at ca. 42 K, (d) Ne at ca. 9 K, (e) He at ca. 4 K. (f) Theoretical harmonic IR spectrum (scaling factor = 0.988) calculated using BP86/def2-TZVP. The two conformers showed the same theoretical IR spectrum. (g) Theoretical anharmonic IR spectrum calculated using same density functional method. A scaling factor of 1.024 was used.

Seven vibrational bands appear in the experimental infrared action spectra. All the experimental spectra show the same number of peaks in the range of 3000 to 3150 cm^{-1}, except for the spectrum obtained upon Ar-tagging, where the last peak is not observed.

During DFT calculations two conformers of the corresponding $Ag(PPh_3)_2^+$ were located: the staggered and the eclipsed conformers. The question of which combination of methods and basis sets provides the best match between theory and experiment for the large organometallic complexes was thoroughly investigated by Reiher's group [40-43]. As a result, we use BP86/def2-TZVP to compute our harmonic IR spectra.

The predicted harmonic IR spectra for the staggered and eclipsed conformers are almost identical. Figure 12 (f) shows the calculated harmonic IR spectrum of the more stable staggered conformer, which was computed to be lower in energy by 0.15 kcal mol^{-1}. The calculated spectrum counts four vibrational bands. We used a scaling factor of 0.988 in order to match the most intense peak on the theoretical spectrum to the absorption band around 3068 cm^{-1} of the experimental spectra. In addition, the BP86/def2-SVP calculations of the tagged complexes confirmed the innocent character of all used tags on the harmonic vibrational spectrum of the $Ag(PPh_3)_2^+$ cation (see Supporting Information).

Next, we performed anharmonic frequency calculations of the $Ag(PPh_3)_2^+$ cation using second-order vibrational perturbation theory (VPT2). In contrast to the harmonic frequency calculations, we obtained different anharmonic vibrational spectra for the different conformers of $Ag(PPh_3)_2^+$. In the corresponding range, the anharmonic IR spectra show five peaks for the staggered, and two for the eclipsed conformer, respectively, presumably because anharmonicity introduces couplings that spread the oscillator strength over previously dark modes. Both spectra are displayed in Figure 12 (g) with a scaling factor of 1.0246.

Overall, the anharmonic spectra seem to reproduce the experiment better, especially the peaks at lower wavenumbers. If we assume both conformers to be present in the ICR cell, nearly all experimental peaks can be assigned. The remaining vibrational bands could arise from further conformations populated at equilibrium, or trapped by rapid cooling. While a more thorough conformational search may lead to a clean identification of all frequency bands, that is not the objective of the present study.

V. DISCUSSION

High background pressure in FT-ICR-MS is unusual because it can perturb the mass spectra of trapped ions. The time domain signal transient is quickly damped to zero due to collisions with the background gas. This leads to a dramatic loss of intensity, especially at higher resolutions. Furthermore, the magnetron radius of trapped ions increase with an increasing number of collisions, causing a loss of excitation efficiency, and, ultimately, a loss of ions and signal intensity [29]. On the other hand, effective cooling of trapped ions, as well as formation of ion-neutral complexes, require a large number of collisions with the buffer gas. A potential workaround for the competing priorities would be the use of a second cryogenic ion trap, such that the

formation of ion-neutral complexes and the excitation/detection are spatially separated from each other. Such setups have been constructed using a hexapole ion trap [19]. Another possibility would be the use of a dual FT-ICR cell [44, 45].

Nevertheless, we profit from a single ICR cell by obtaining steady-state conditions for signal intensities of tagged and untagged species. In a pulsed laser experiment usually the transient changes in a mass spectrum are recorded after each laser shot, and then averaged over some total number of shots. We, in contrast, monitor the difference between the steady-state distribution of ions, measured with or without laser irradiation. For the measurement of the distribution of trapped ions, we average the FID over a specified number of excitation pulses (usually 5–10 pulses) in the FT-ICR cell for each steady-state distribution. While we use a pulsed laser source, the method should work with either pulsed or continuous lasers. We do not have to eject ions after each duty cycle. We "reuse" the same ions multiple times, and the laser may be left unsynchronized with other timed events of the experiment; in particular, the laser is not synchronized with the train of excitation pulses to the FT-ICR cell. This potentially leads to a shorter duty cycle because the cell can be constantly refilled. Typically, one data point takes ca. 1–2 minutes to record. For example, to record a spectrum like the one shown in Figure 12 (b) with 150 data points required ca. three hours and twenty minutes. Optimization of measurement time was one of the principal design targets of the present instrument.

Usually, in FT-ICR MS, the ions must be excited to a larger cyclotron radius for the detection of image currents on the detection plates. In principle, larger cyclotron radii lead to larger signal intensities. However, the kinetic energy of the ions increases with a larger cyclotron radius as well, meaning, necessarily larger collision energies. Higher collision energies, to continue the logic, lead to enhanced cleavage of weak bonds in the ion-neutral complexes formed in the collision cell. Therefore, for the largest possible fraction of tagged ions, we find that the excitation amplitude should be kept low.

Undesired magnetron motion at high pressures in FT-ICR-MS can be decreased by a two-plate azimuthal quadrupolar excitation pulse [36] prior to the excitation of trapped ions. Such an axialization pulse leads to an interconversion of magnetron and cyclotron motion. If applied for multiple conversion cycles, it helps to reduce the magnetron radius and improve the excitation efficiency. In our case, better quality mass spectra could be obtained by introducing only a very short axialization pulse when no actual dipolar excitation pulse is applied. In some experiments it seemed to be easier to observe ion-neutral complexes by the use of axialization pulses only. The resolution of the mass spectra obtained this way remains moderate at such high pressures, but clearly good enough to identify all the species present in the ion trap with baseline separation of isotopic species.

In addition, even if the quality of the observed mass spectra is low when a pure dipolar excitation pulse is applied, the absorption of infrared radiation clearly changes the appearance of the mass spectrum, the monitoring of which produces an infrared spectrum. We do find that poor quality mass spectra may lead to better infrared action spectra in terms of the signal-to-noise ratio, because the change of peak intensities upon irradiation is more distinct. In such cases, the use of a short axialization pulse, to produce a better mass spectrum, can be useful to prove the identity of the trapped analytes. Table II gives an overview of the consequences observed by applying different excitation modes.

TABLE II: observed trends for the effect of different excitation modes for the quality of mass spectra and infrared action spectra.

	dipolar excitation	quadrupolar excitation
MS	quality often worse, ion-neutral complexes not always visible	better quality, ion-neutral complexes more easily visualized
IR	absorption of photons usually lead to a clear change in the mass spectrum	absorption of photons does not always change the mass spectrum much

Broadband two-plate azimuthal quadrupolar excitation mode seems to be a softer way to excite trapped ions under the "high" pressure conditions needed to form tagged ions efficiently. We do not entirely understand why, but action spectroscopy is nevertheless more difficult using this excitation mode in some instances.

Ions of different masses show different behaviors in the ICR trap. Lighter ions generally profit from higher resolutions at short detection times. On the other hand, neutral tagging seems to be more difficult with lighter ions. For a more efficient tagging of lighter ions, the excitation time should be kept shorter than 2 ms. Experiments on different light ions in the range of 100–300 amu have shown, that excitation times of 50 microseconds lead to more intense signals of the tagged species. Larger molecules usually form adducts with neutral gases at higher temperatures and lower pressures than smaller molecules and longer excitation pulses can be applied. The high pressures used in our experiments are more problematic for the detection of larger ions due to the longer detection times. However, ions with m/z ratios above 1000 could be tagged and probed with our instrument without problems.

We observe that heavier buffer gases show a more severe impact on the quality of the mass spectra than lighter buffer gases at the same number density, as one would expect. Nitrogen and hydrogen seem to interact more strongly with the analyte, again as one would expect. The number of messenger particles on the analyte as well as the signal intensities of tagged species are higher than those observed with rare gases. For the rare gases, it is more difficult to observe ion-neutral complexes, the lighter the messenger is. Ion-neutral complexes with helium are the most difficult to observe. Figure 10 shows that a reasonable fraction of the He-tagged species can be observed at the lowest possible temperature. Higher buffer gas pressures generally lead to a larger signal intensity of the ion-helium complex relative to the signal intensity of the untagged ion. However, the overall signal intensity rapidly decreases with an increasing background pressure. With these two countervailing trends, we take a compromise where the

maximum intensity of the tagged species can be detected at a buffer gas background pressure of ca. 3×10^{-8} mbar.

All infrared action spectra obtained with different sorts of neutral tags show the same number of absorption bands and, in general, the locations of the absorption bands seem to be largely independent from the messenger species (Figure 12). Only the spectra recorded with N_2 and Ar deviate slightly from the other action spectra. In case of the Ar-tagging experiment, the peak at 3100 cm^{-1} does not loom out of the background noise, although one might claim that it still could be present. In the spectrum recorded with N_2, the vibrational band at 3089 cm^{-1} appears with a shoulder on the side of lower wavenumbers. In addition, the peak around 3068 cm^{-1} appears at a slightly higher wavenumber.

Theoretical assignment of the experimentally observed bands at 3100 cm^{-1} as well as 3020 and 3025 cm^{-1} is difficult for harmonic calculated IR spectra. To match all bands with the anharmonic IR spectra, one must assume that both conformers, the staggered and the eclipsed, are present in the ion trap. The energy difference between the two conformers is negligible, so, given the expected accuracy of the DFT calculations, the prospect of a mixed population, even at equilibrium at cryogenic temperatures, is plausible. In this case, the peaks observed in the experimental spectra around 3043, 3068, 3078 and 3078 cm^{-1} would then be ca. 12 cm^{-1} shifted from the predicted frequency. At this point, we have to conclude that we do not have enough data to make the correct assignment of all the experimentally observed vibrations without further experiments, even though the qualitative reproduction of the experimental spectra by the scaled, anharmonic calculations is satisfactory. Given the difference between the harmonic and anharmonic predicted spectra, we would presume that the additional peaks are most likely due to anharmonic coupling to dark modes [46].

VI SUMMARY

We have designed a new instrument for the infrared action spectroscopy of cold ions in the gas phase that operates with a cold FT-ICR cell. Ion-neutral complexes with different gases, including helium, can be detected. The conditions for successful formation of ion-He complexes are explored. Using optimized trapping conditions, infrared action spectra of a suitable model complex with different messenger species are recorded successfully and compared to each other and to theoretically predicted vibrational spectra.

SUPPLEMENTARY MATERIAL

See the Supplementary Material for the Labview control diagrams for the instrument, procedures and data for the estimation of the temperature and pressure in the ICR cell, and details of the quantum chemical calculations.

ACKNOWLEDGEMENTS

We gratefully acknowledge support of this work by the Schweiz. Nationalfonds and ETH Zürich. The authors would like to thank Christoph Bärtschi for his most exact fabrication of hardware parts and Heinz Benz for preparing solutions for electronic requirements of our instrument. Armin Limacher's efforts in the construction and maintenance of the instrument are gratefully acknowledged.

REFERENCES

1. J.-C. Jiang, Y.-S. Wang, H.-C. Chang, S. H. Lin, Y. T. Lee, G. Niedner-Schatteburg and H.-C. Chang, J. Am. Chem. Soc. **122**, 1398-1410 (2000).
2. J. M. Bakker, L. M. Aleese, G. Meijer and G. von Helden, Phys. Rev. Lett. **91**, 203003 (2003).
3. M. A. Duncan, Int. Rev. Phys. Chem. **22**, 407-435 (2003).
4. W. H. Robertson and M. A. Johnson, Ann. Rev. Phys. Chem. **54**, 173-213 (2003).
5. B. C. Dian, G. M. Florio, J. R. Clarkson, A. Longarte and T. S. Zwier, J. Chem. Phys. **120**, 9033-9046 (2004).
6. J. Oomens, N. Polfer, D. T. Moore, L. van der Meer, A. G. Marshall, J. R. Eyler, G. Meijer and G. von Helden, Phys. Chem. Chem. Phys. **7**, 1345-1348 (2005).
7. T. R. Rizzo, J. A. Stearns and O. V. Boyarkin, Int. Rev.in Phys. Chem. **28**, 481-515 (2009).
8. T. Baer and R. C. Dunbar, J. Am. Soc. Mass Spectrom. **21**, 681-693 (2010).
9. J. Roithova, Chem. Soc. Rev. **41**, 547-559 (2012).
10. Y. S. Wang, C. H. Tsai, Y. T. Lee, H. C. Chang, J. C. Jiang, O. Asvany, S. Schlemmer and D. Gerlich, J. Phys. Chem. A **107**, 4217-4225 (2003).
11. A. Alili, J. Andre and F. Vedel, Phys. Scr. **T22**, 325-328 (1988.).
12. W. M. Itano, J. C. Bergquist, J. J. Bollinger and D. J. Wineland, Phys. Scr. **T59**, 106-120 (1995).
13. N. R. Hutzler, H.-I. Lu and J. M. Doyle, Chem. Rev. **112**, 4803-4827 (2012).
14. H.-B. Oh, C. Lin, H. Y. Hwang, H. Zhai, K. Breuker, V. Zabrouskov, B. K. Carpenter and F. W. McLafferty, J. Am. Chem. Soc. **127**, 4076-4083 (2005).
15. K. R. Asmis and J. Sauer, Mass Spectrom. Rev. **26**, 542-562 (2007).
16. A. Svendsen, U. J. Lorenz, O. B. Boyarkin and T. Rizzo, Rev. Sci. Instrum. **81**, 073107 (2010).
17. M. Z. Kamrath, R. A. Relph, T. L. Guasco, C. M. Leavitt and M. A. Johnson, Int. J. Mass Spec. **300**, 91-98 (2011).
18. J. Jašík, J. Žabka, Roithová, J. and D. Gerlich, Int. J. Mass Spec. **354–355**, 204-210 (2013).
19. J. Mohrbach, J. Lang, S. Dillinger, M. Prosenc, P. Braunstein and G. Niedner-Schatteburg, J. Mol. Spec. **332** 103-108 (2017).
20. C. J. Johnson, A. B. Wolk, J. A. Fournier, E. N. Sullivan, G. H. Weedle and M. A. Johnson, J. Chem. Phys. **140**, 221101 (2014).
21. O. Dopfer, S. A. Nizkorodov, M. Meuwly, E. J. Bieske and J. P. Maier, Chem. Phys. Lett. **260**, 545-550 (1996).
22. S. A. Nizkorodov, D. Roth, R. V. Olkhov, J. P. Maier and O. Dopfer, Chem. Phys. Lett. **278**, 26-30 (1997).
23. D. Roth, S. A. Nizkorodov, J. P. Maier and O. Dopfer, J. Chem. Phys. **109**, 3841-3849 (1998).
24. O. Dopfer, R. V. Olkhov, D. Roth and J. P. Maier, Chem. Phys. Lett. **296**, 585-591 (1998).

25. M. Brümmer, C. Kaposta, G. Santambrogio and K. R. Asmis, J. Chem. Phys. **119**, 12700-12703 (2003).
26. N. Dietl, T. Wende, K. Chen, L. Jiang, M. Schlangen, X. Zhang, K. R. Asmis and H. Schwarz, J. Am. Chem. Soc. **135**, 3711-3721 (2013).
27. J. Jašík, D. Gerlich and J. Roithová, J. Am. Chem. Soc. **136**, 2960-2962 (2014).
28. M. B. Comisarow and A. G. Marshall, Chem. Phys. Lett. **25**, 282-283 (1974).
29. A. G. Marshall, C. L. Hendrickson and G. S. Jackson, Mass Spectrom. Rev. **17**, 1-35 (1998).
30. S. Dillinger, J. Mohrbach, J. Hewer, M. Gaffga and G. Niedner-Schatteburg, Phys. Chem. Chem. Phys. **17**, 10358-10362 (2015).
31. S. Dillinger, M. P. Klein, A. Steiner, D. C. McDonald, M. A. Duncan, M. M. Kappes and G. Niedner-Schatteburg, J. Phys. Chem. Lett. **9**, 914-918 (2018).
32. H. Raimbault-Hartmann, D. Beck, G.Bollen, M. König, H.-J. Kluge, E. Schark, J. Stein, S. Schwarz and J. Szerypo, Nucl. Instrum. Methods Phys. Res. B **126**, 378-382 (1997).
33. A. G. Marshall, T.-C. L. Wang and T. L. Ricca, J. Am. Chem. Soc. **107**, 7893-7897 (1985).
34. S. Guan and A. G. Marshall, Int. J. Mass Spectrom. Ion Proc. **157-158**, 5-37 (1996).
35. L. Schweikhard and A. G. Marshall, J. Am. Soc. Mass Spectrom. **4**, 433-452 (1993).
36. G. S. Jackson, C. L. Hendrickson, B. B. Reinhold and A. G. Marshall, Int. J. Mass Spectrom. Ion Proc. **165-166**, 327-338 (1997).
37. M. J. Frisch, G. W. Trucks, H. B. Schlegel, G. E. Scuseria, M. A. Robb, J. R. Cheeseman, G. Scalmani, V. Barone, B. Mennucci, G. A. Petersson, H. Nakatsuji, M. Caricato, X. Li, H. P. Hratchian, A. F. Izmaylov, J. Bloino, G. Zheng, J. L. Sonnenberg, M. Hada, M. Ehara, K. Toyota, R. Fukuda, J. Hasegawa, M. Ishida, T. Nakajima, Y. Honda, O. Kitao, H. Nakai, T. Vreven, J. A. Montgomery, J. E. Peralta, F. Ogliaro, M. Bearpark, J. J. Heyd, E. Brothers, K. N. Kudin, V. N. Staroverov, R. Kobayashi, J. Normand, K. Raghavachari, A. Rendell, J. C. Burant, S. S. Iyengar, J. Tomasi, M. Cossi, N. Rega, J. M. Millam, M. Klene, J. E. Knox, J. B. Cross, V. Bakken, C. Adamo, J. Jaramillo, R. Gomperts, R. E. Stratmann, O. Yazyev, A. J. Austin, R. Cammi, C. Pomelli, J. W. Ochterski, R. L. Martin, K. Morokuma, V. G. Zakrzewski, G. A. Voth, P. Salvador, J. J. Dannenberg, S. Dapprich, A. D. Daniels, Farkas, J. B. Foresman, J. V. Ortiz, J. Cioslowski and D. J. Fox, (Wallingford CT, 2009).
38. V. Barone, J. Chem. Phys. **122**, 014108 (2005).
39. V. Barone, J. Bloino, C. A. Guido and F. Lipparini, Chem. Phys. Lett. **496**, 157-161 (2010).
40. M. Reiher, V. Liégeois and K. Ruud, J. Phys. Chem. A **109**, 7567-7574 (2005).
41. J. Neugebauer, M. Reiher and B. A. Hess, J. Chem. Phys. **117**, 8623-8633 (2002).
42. L. Yu, C. Greco, M. Bruschi, U. Ryde, L. De Gioia and M. Reiher, Inorg. Chem. **50**, 3888-3900 (2011).
43. J. Neugebauer and B. A. Hess, J. Chem. Phys. **118**, 7215-7225 (2003).
44. M. V. Gorshkov, L. Pasa-Tolić, J. E. Bruce, G. A. Anderson and R. D. Smith, Anal. Chem. **69**, 1307-1314 (1997).
45. J. R. Gord and B. S. Freiser, Anal. Chim. Acta **225**, 11-24 (1989).
46. C. M. Leavitt, A. F. DeBlase, C. J. Johnson, M. van Stipdonk, A. B. McCoy and M. A. Johnson, J. Phys. Chem. Lett. **4**, 3450-3457 (2013).

Supplementary Information

A) FT-ICR MS LabView Codes

LabView codes are written for the exciation and detection of ions trapped in the ICR cell. The user defines the mass window and the excitation time and the LabView program will convert it to the excitation pulse using the stored waveform inverse Fourier transform (SWIFT) approach. The exciation pulse is applied to the excitation electrodes via two 14 bit arbitrary waveform generators (AWGs). The detected time domain signal is digitized by a 14 bit digitizer. The LabView code performs a Fourier transform to the signal and converts the obtained frequency spectrum to a mass spectrum. The LabView block diagram of the exciation/detection routine is shown and explained in the following pictures.

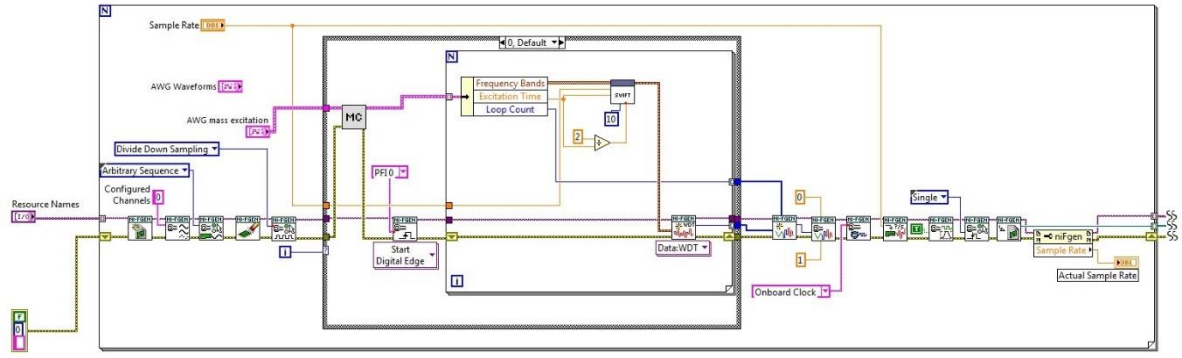

FIG. S1: LabView block diagram of the exciation routine used in our instrument. The settings define the output of one of the 14-bit arbitrary waveform generators (AWG) that is connected to one of the excitation electrodes.

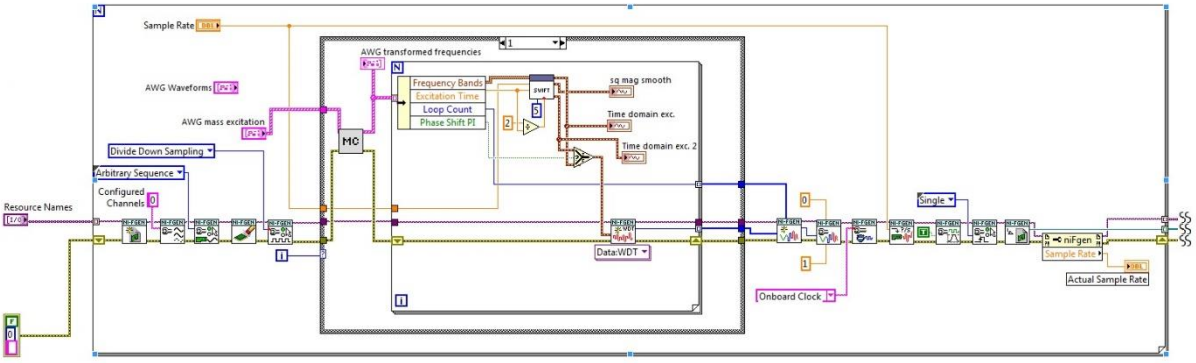

FIG. S2: LabView block diagram of the exciation routine used in our instrument. The settings define the output of the second 14-bit AWG that is connected to the other excitation electrode. For a dipolar excitation, a phase shift of 180° has to be applied.

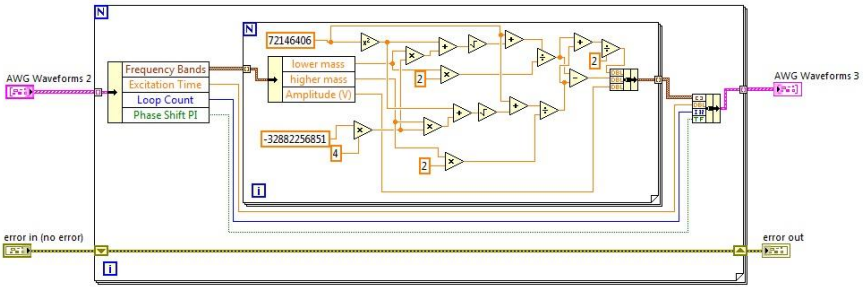

FIG. S3: LavView block diagram of the “MC”-subVI used for the conversion of the user defined excitation mass range to the frequency range for the SWIFT-excitation

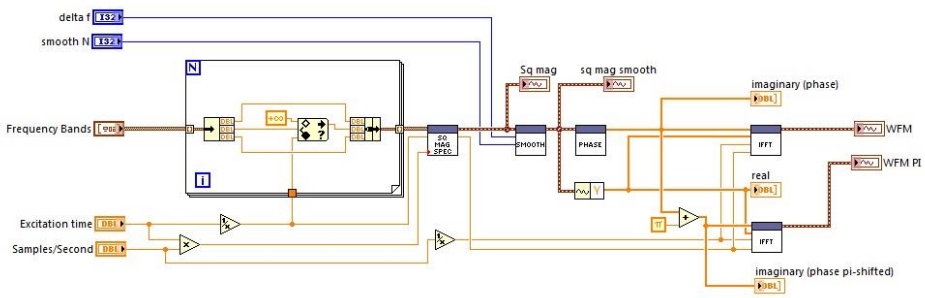

FIG. S4: LabView block diagram of the "SWIFT"-subVI used for the generation of the excitation waveforms. The user-defined square magnitude profile is smoothed, phase modulated and inverse-Fourier transformed to yield the SWIFT excitation waveforms.

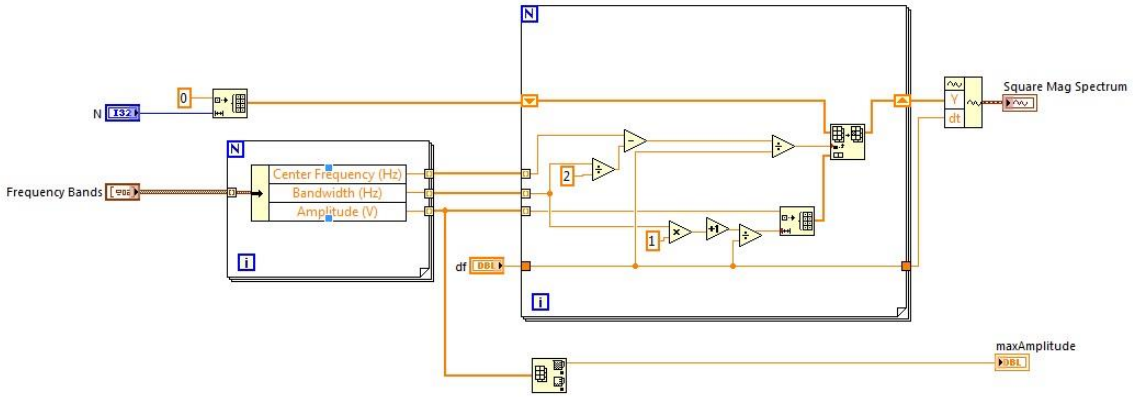

FIG. S5: LabView block diagram of the "SQ MAG SPEC"-subVI used for the generation of the user defined square magnitude spectrum for the desired exciation band.

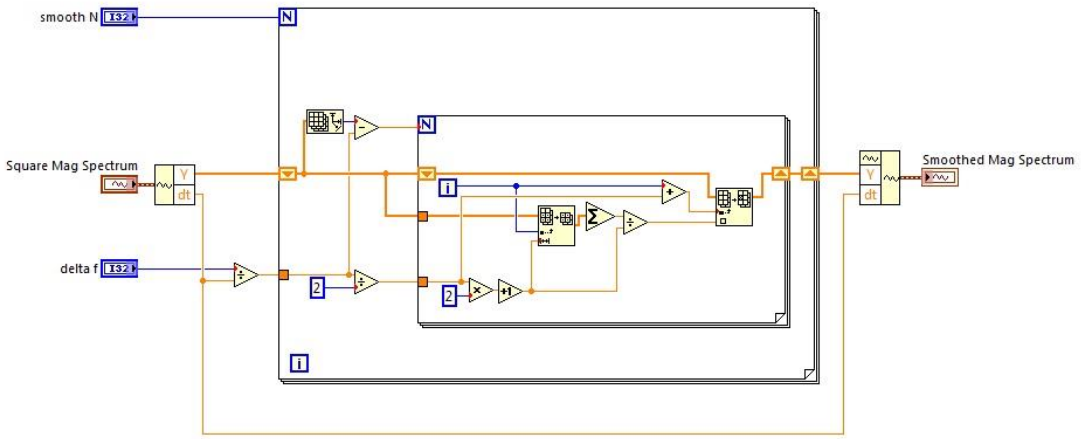

FIG. S6: LabView block diagram of the "SMOOTH"-subVI used for the smoothing of the square magnitude spectrum.

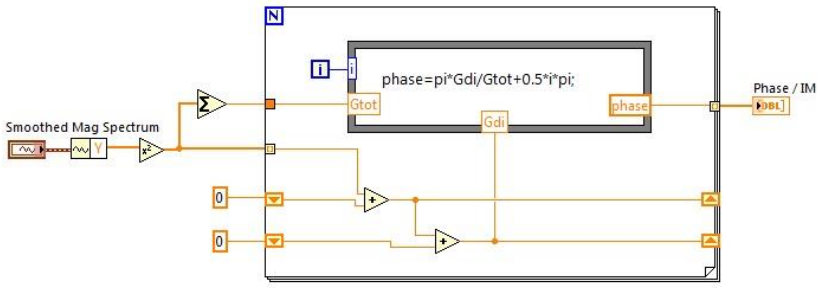

FIG. S7: LavView block diagram of the "PHASE"-subVI used for the phase modulation of the smoothed magnitude spectrum.

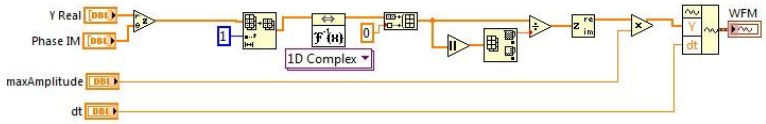

FIG. S8: Lab View block diagram of the "IFFT"-subVI used for the inverse Fourier-transform of the mass window to the corresponding excitation waveform.

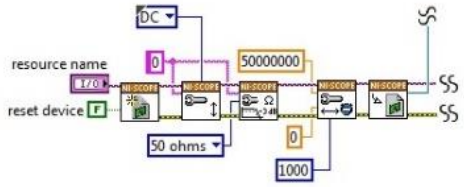

FIG. S9: LabView block diagram for the initialization of the 14 bit digitizer used for the signal detection.

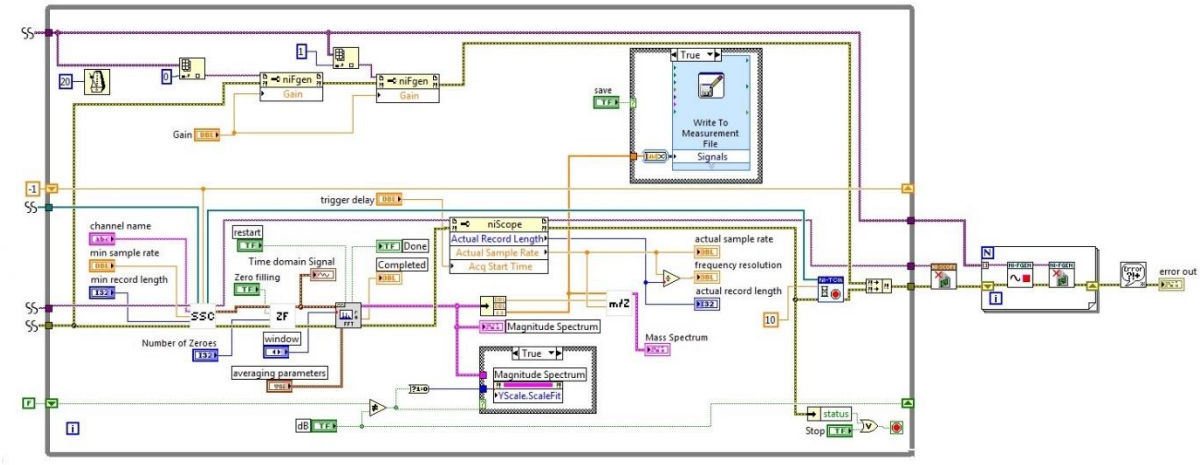

FIG. S10: LabView block diagram for the detection routine. The time domain signal, digitized by the 14 bit digitizer is zero-filled and Fourier transformed to a frequency spectrum and then converted to a mass spectrum.

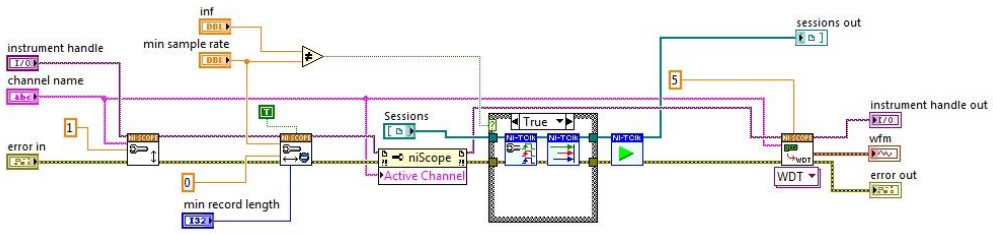

FIG. S11: LabView block diagram fort he "SSC"-subVI used for the on-line digitizer-settings during the experiment.

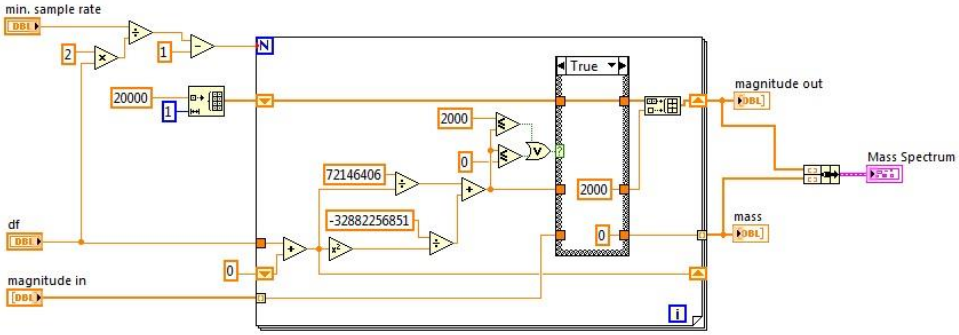

FIG. S12: LabView block diagram of the "m/z"-subVI used for the conversion of the frequency spectrum to a mass spectrum.

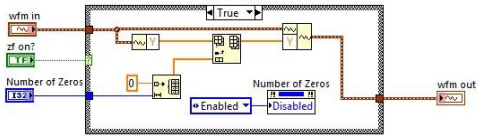

FIG. S13: LabView block diagram for the "ZF"-subVI for the zero-filling of the time domain signal.

B) LabView block diagrams for the laser scan

The LabView code for the frequency scanning with the laser is written using an eventhandler and a state machine. Basically, the user specifies the starting wavelength for the scan and the stepsize. The software then adjusts the diffraction grating of the dye laser and the angles of the BBO- and KTA crystals such that the desired output frequency is generated by the laser system at every step during the scan.

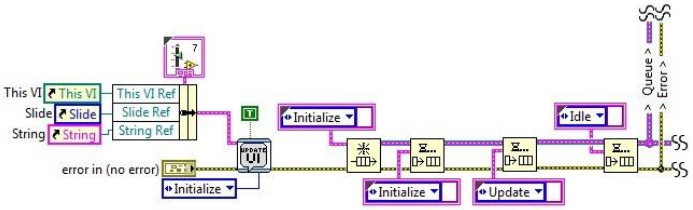

FIG. S14: Block diagram for the initialization oft he event handler and the state machine fort he laser scan software.

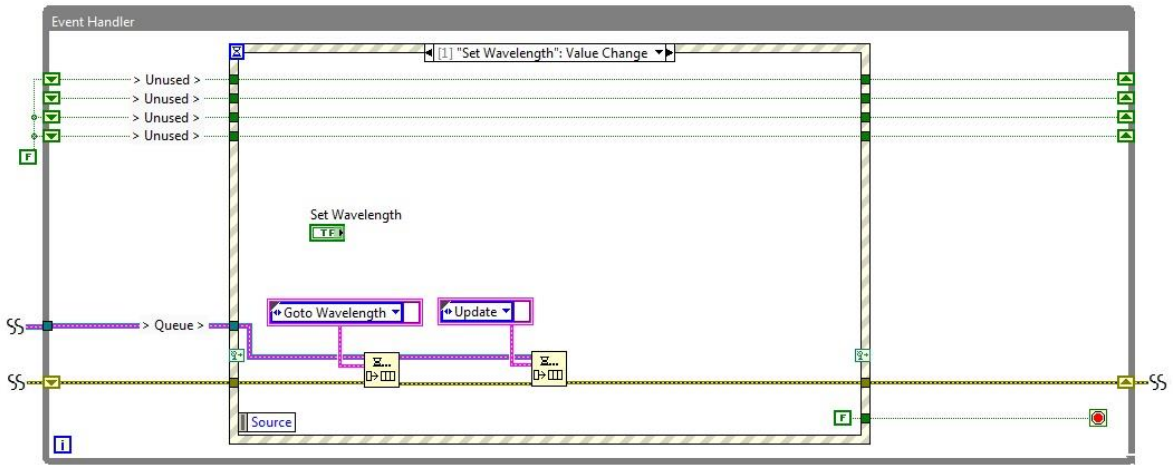

FIG. S15: Event handler structure used for the laser scan software. The “Set Wavelength” event triggers the adjustment of the diffraction grating of the dye laser and the angles for the frequency mixing crystals to obtain the desired wavelengths. Similar events set the step size and shift the laser wavelength one step to red or blue respectively.

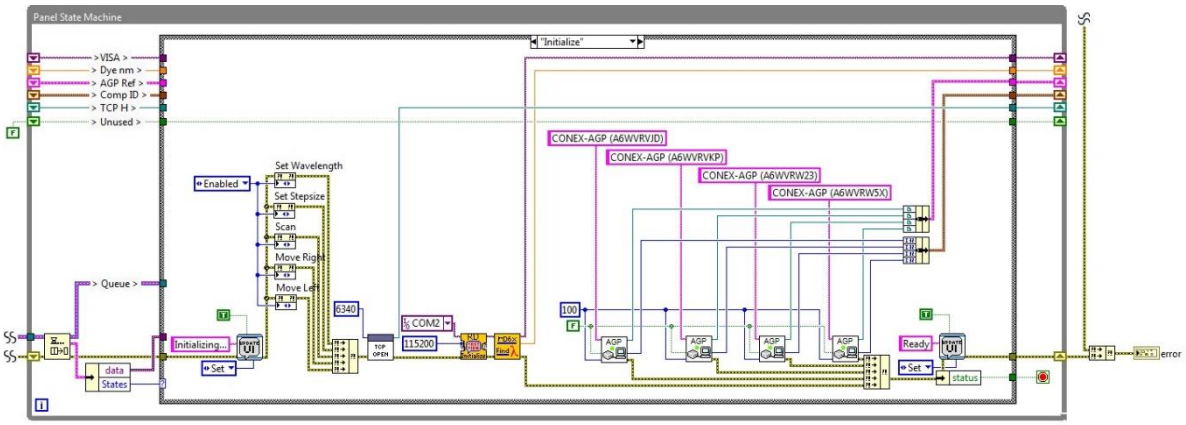

FIG. S16: State machine structure used for the laser scan software. The dye laser motor and the rotation mounts for the four mixing crystals is initialized in this state. The subVI’s for controlling of the AGP rotation mounts are supplied by National Instruments.

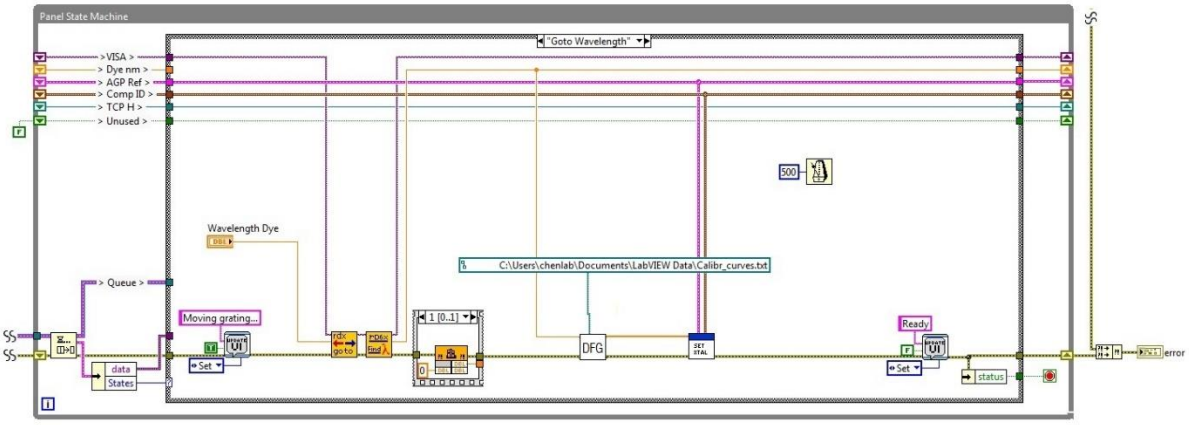

FIG. S17: Block diagram for the state in which the dye laser motor and the rotation mounts for the four mixing crystals are adjusted. The subVI’s for the adjustment of the dye laser oscillator diffraction grating are provided by Radiant Dyes.

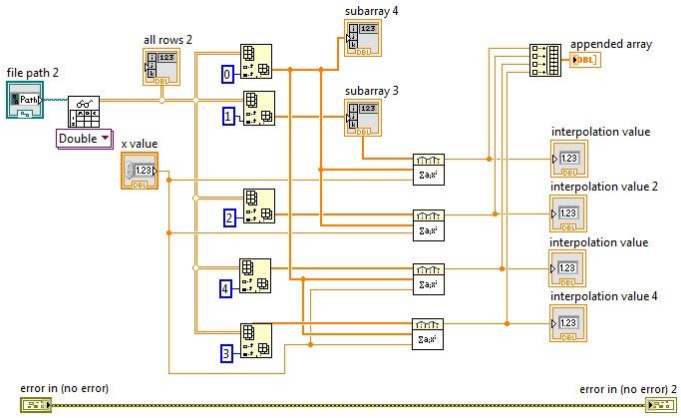

FIG. S18: LabView block diagram of the “DFG”-subVI used for the determination of the correct angles for the mixing cristals. The values are obtained by interpolation of points given in a calibration file.

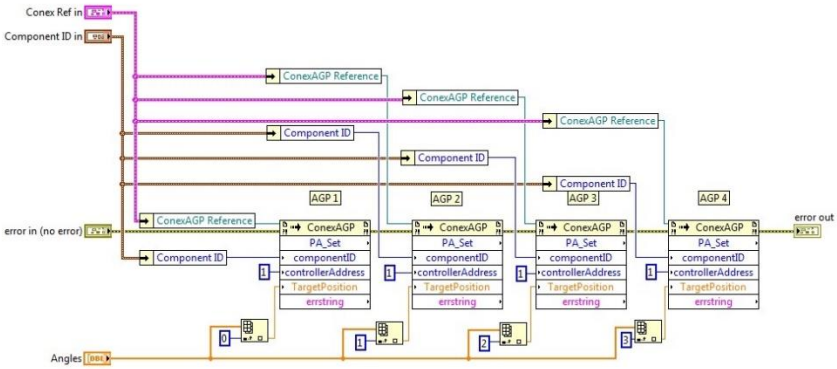

FIG. S19: LabView block diagram of the “Set Xtal”-subVI used for the adjustment of the mixing crystal angles.

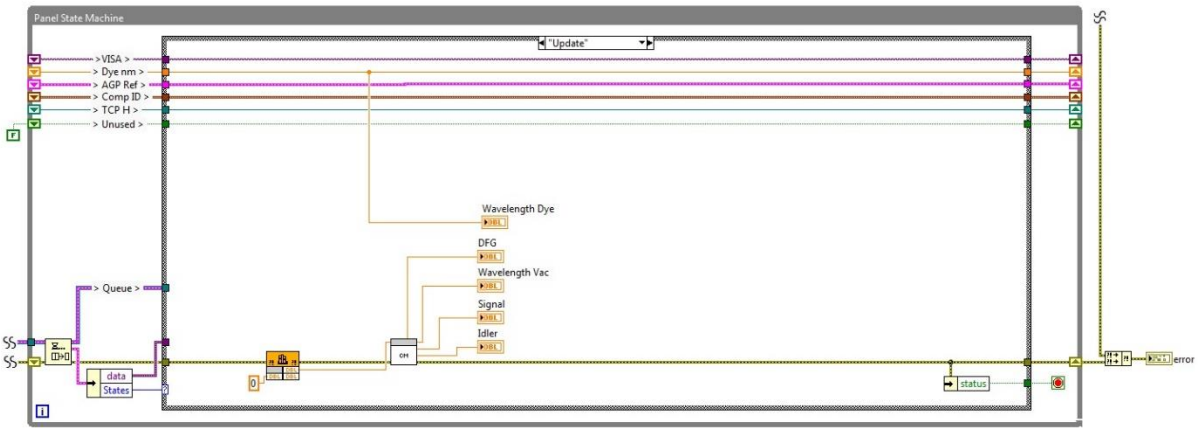

FIG. S20: Block diagram for the state used to read the set output wavelength of the dye laser in air. The dye laser wavelength is converted to the wavelength in vacuum and the frequencies obtained by frequency mixing. The “idler” wave is used for ion spectroscopy.

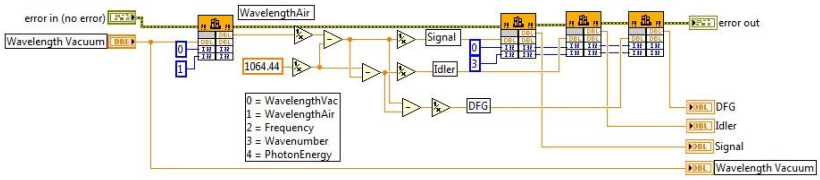

FIG. S21: LabView block diagram of the “CM”-subVI used for the conversion of the set air wavelength of the dye laser to the corresponding vacuum wavelength and the wavelengths resulting from the two-stage frequency mixing.

C) Cell temperature

The temperature of the instrumental setup is monitored at four different places in the presented instrument. An overview is given in FIG. S22.

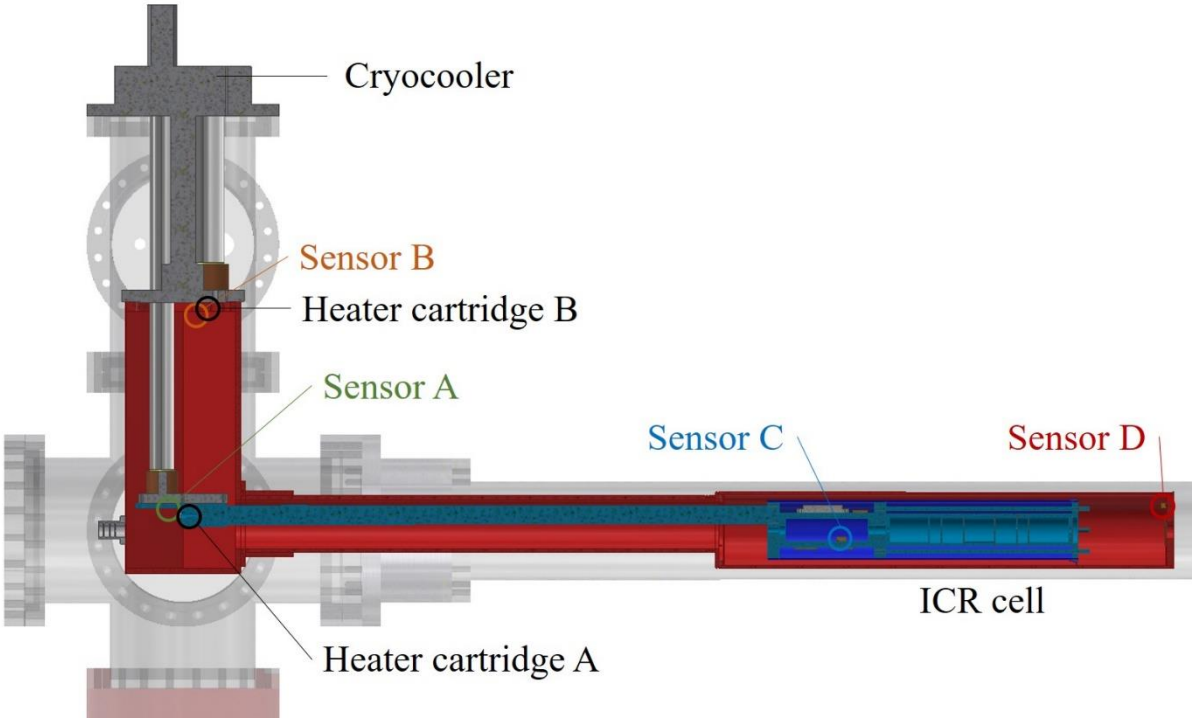

FIG. S22: Schematic drwaing of the ICR cell and the cryocooler. The temperature is measured with Sensors A through D.

The Temperatures during the cooldown of the ICR cell have been recorded and are shown in FIG. S23.

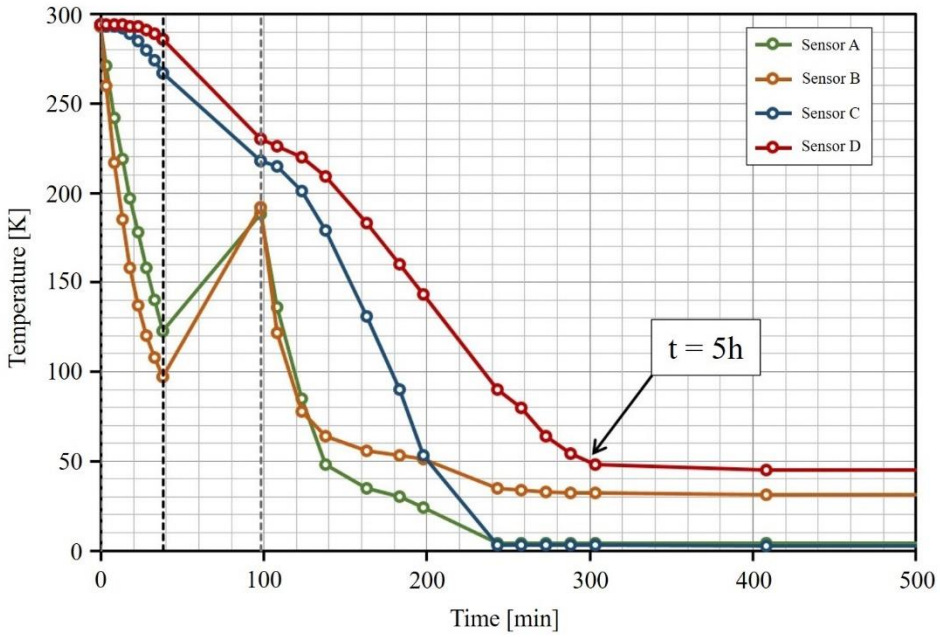

FIG. S23: Temperatures displayed by the four sensors as a function of time during the cooldown of the instrument. The cryocooler was disabled after ca. 40 min. (vertical black dashed line) in order to reduce the temperature gradients between warm and cold parts of the instrument. After ca. 100 min. the cryocooler was switched on again (vertical gray dashed line). The final temperatures were reached after 5 h.

Final temperatures were reached after 5 h including a 1 h period during which the cryocooler was switched off for safety reasons. Temperature changes in the range of 4 – 50 K (Sensor C) are usually established in a few minutes.

D) Cell pressure

The time averaged pressure within the ICR cell has been tried to estimate by the gas-flow through a simplified model of the ion trap. With the specified pumping speed S (650 L/s) of the turbomolecular pump and the measured the background pressure P (3×10^{-8} mbar = 3×10^{-5} Ba), the throughput Q can be determined:

$$Q = SP = 650\frac{L}{s} \cdot 3 \cdot 10^{-5}\frac{g}{cm \cdot s^2} = 0.0195$$

In addition, we expect a laminar gas flow and the following expression to be true:

$$Q = C\Delta P$$

With ΔP, the pressure difference between the cell and the background pressure and C, the conductivity of the cell. The conductivity depends on the geometry and the temperature of the gas and the total conductivity can be modeled as:

$$\frac{1}{C} = \frac{1}{C_t} + \frac{1}{C_a} + \cdots$$

Where Ct is the conductivity of a tube and Ca is the conductivity of an aperture.

$$C_t = 3.81\left(\frac{T}{M}\right)^{1/2}\frac{D^3}{L}$$

$$C_a = 2.86\left(\frac{T}{M}\right)^{1/2} 4\,r^2$$

T is the temperature, r is the inner radius, D is the inner diameter, L is the length of the tube and M is the molecular mass of the gas. The calculations are all conducted in CGS units (length in cm, mass in g, time in s, temperature in K and conductivity in L/s). The compounds taken into account for the modeling of C are sketched in Figure 14.

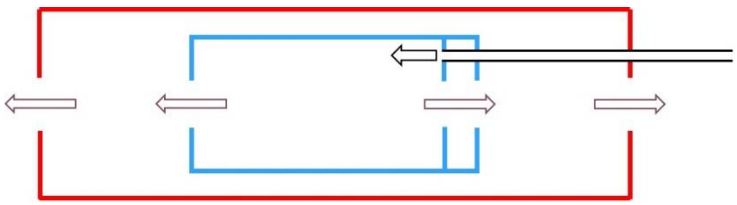

FIG. S24: Model oft he cell including the inner radiation shield. The buffer gas is flowing into the cell through a small steel tube (black). The gas flow out of the cell leads through the cell itself, treated as a tube and several apertures in the cell (blue) and the outer radiation shield (red).

Using He at 4 K as background gas, the following partial conductivities are determined:

C1: $3.81\left(\frac{4}{4}\right)^{1/2}\frac{2.8^3}{19.3} = 4.33$ (cell, treated as a tube)

C2: $2.86\left(\frac{4}{4}\right)^{1/2} 4 \cdot 0.3^2 = 1.03$ (apertures in the cell)

C3: $2.86\left(\frac{50}{4}\right)^{1/2} 4 \cdot 0.3^2 = 3.64$ (apertures in the radiation shield)

Other conductivity contriubutions are much larger and do not contribute much to the total conductivity which is determined as:

$$\frac{1}{C} = \frac{1}{4.33} + \frac{1}{1.5 * 1.03} + \frac{1}{2 * 3.64} = 1.0$$

With C = 1, the pressure difference can be calculated:

$$\Delta p = \frac{Q}{C} = \frac{0.0195}{1} = 0.02\ Ba = 2 \cdot 10^{-5}\ mbar$$

The background pressure is much smaller than the pressure difference, such that the pressure within the cell should be at least 2×10^{-5} mbar or around three orders of magnitude larger than the background pressure. Temporal pressure fluctuations have not been taken into account in this calculation and the temporal maximum pressure could be considerably larger than the time averaged pressure since the buffer gas is introduced through a pulsed valve with a short opening time.

Reference:

A. Roth, Vacuum Technology, North-Holland Verlag, third, updated and enlarged edition, 1990.

E) Infrared spectra

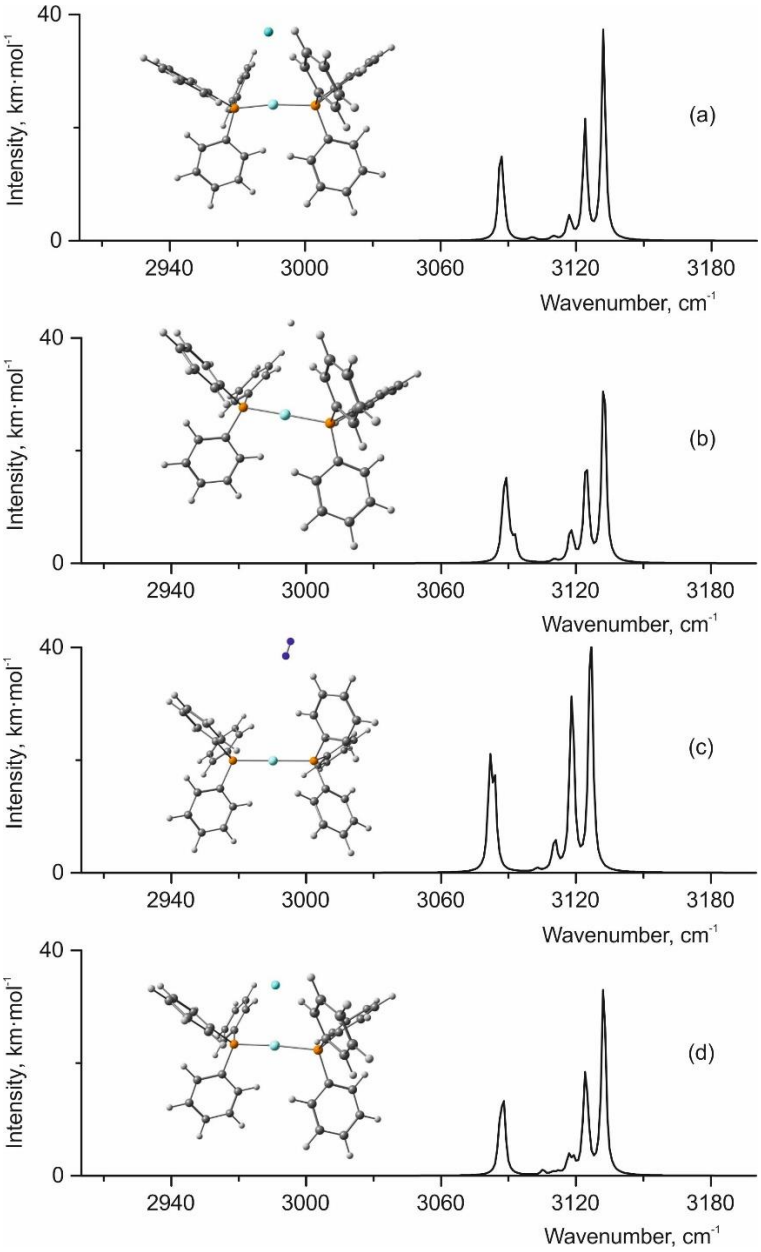

FIG. S25: Theoretically predicted spectra of the eclipsed conformer of the $Ag(Ph_3P)_2^+$ cation with: a) Ar, b) He, c) N2 and d) Ne used as neutral tags. The spectra are calculated with BP86/def2-SVP level of theory, the frequencies are not scaled.

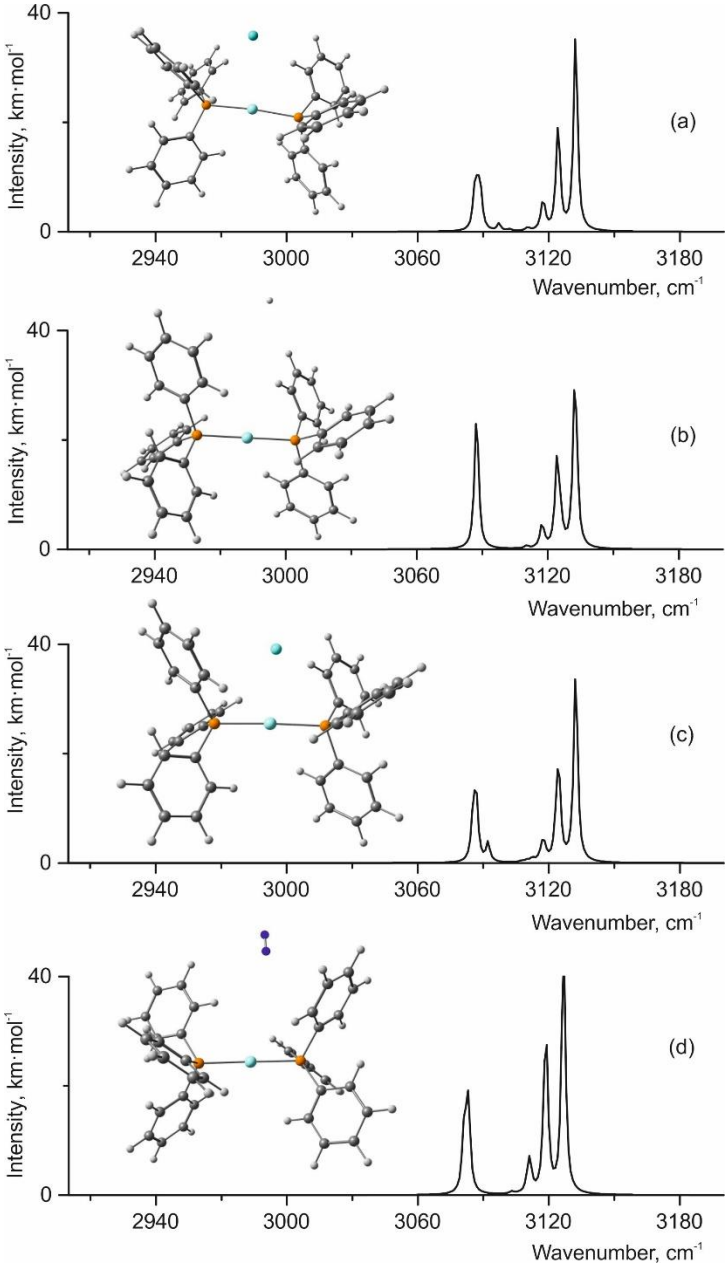

FIG. S26. Theoretically predicted spectra of the staggered conformer of the $Ag(Ph_3P)_2^+$ cation with: a) Ar, b) He, and c) Ne used as neutral tags. The spectra are calculated with BP86/def2-SVP level of theory, the frequencies are not scaled.

F) Optimized geometries

Table S1. The BP86/def2-TZVP optimized gas-phase geometries. For each structure, the number of atoms, the structure name and vibrational zero point energy (in Hartree) are given, followed by the Cartesian coordinates of each atom (in Å).

69

$Ag(Ph_3P)_2^+$_eclipsed Energy = -2219.608673

P	2.400643000	-0.101149000	0.084622000
Ag	0.004002000	-0.214905000	-0.078590000
P	-2.396344000	-0.273891000	-0.225053000
C	-3.049810000	1.075776000	-1.271623000
C	-4.125757000	0.882422000	-2.153038000
C	-4.603501000	1.951531000	-2.917164000

C	-4.016717000	3.215081000	-2.804986000
C	-2.943026000	3.412312000	-1.929486000
C	-2.455882000	2.346834000	-1.171024000
C	3.043590000	1.528280000	-0.441471000
C	2.461146000	2.146094000	-1.562595000
C	2.942949000	3.374338000	-2.017741000
C	3.999865000	4.002639000	-1.349835000
C	4.575355000	3.398257000	-0.228587000
C	4.102521000	2.163677000	0.226823000
C	3.234549000	-1.346778000	-0.962146000
C	2.686516000	-2.640143000	-1.033320000
C	3.309297000	-3.625536000	-1.800953000
C	4.475502000	-3.325043000	-2.513611000
C	5.019002000	-2.038744000	-2.453915000
C	4.404180000	-1.049791000	-1.680278000
C	3.000908000	-0.370914000	1.791287000
C	4.131411000	-1.156943000	2.067083000
C	4.560236000	-1.325185000	3.387305000
C	3.870470000	-0.710225000	4.435576000
C	2.742698000	0.073310000	4.165974000
C	2.304166000	0.237292000	2.851264000
C	-3.042513000	-1.836153000	-0.922983000
C	-4.167305000	-2.476014000	-0.378265000
C	-4.642339000	-3.661062000	-0.947807000
C	-4.003714000	-4.210955000	-2.062432000
C	-2.881862000	-3.577344000	-2.609001000
C	-2.397165000	-2.398926000	-2.039023000
C	-3.184047000	-0.081254000	1.414641000
C	-4.315171000	0.728541000	1.605654000
C	-4.893518000	0.832920000	2.874411000
C	-4.352541000	0.130474000	3.954702000
C	-3.225119000	-0.677574000	3.769517000
C	-2.637842000	-0.778462000	2.507393000
H	1.630175000	1.663230000	-2.084252000
H	4.554864000	1.698729000	1.104498000
H	2.488759000	3.844985000	-2.891431000
H	5.396965000	3.887984000	0.297060000
H	4.371286000	4.966755000	-1.701416000
H	1.771050000	-2.877946000	-0.484568000
H	4.832058000	-0.046653000	-1.640802000
H	2.880076000	-4.627832000	-1.848592000
H	5.926100000	-1.800441000	-3.012088000
H	4.957445000	-4.093779000	-3.120099000
H	4.674724000	-1.642366000	1.254642000
H	1.417824000	0.844404000	2.648282000
H	5.437748000	-1.940120000	3.594641000
H	2.199285000	0.552261000	4.982346000
H	4.207960000	-0.844606000	5.464701000
H	-4.670425000	-2.053179000	0.492642000
H	-1.516205000	-1.912511000	-2.466400000
H	-5.515570000	-4.154196000	-0.517215000
H	-2.379025000	-4.005625000	-3.477835000
H	-4.376548000	-5.136450000	-2.504621000
H	-1.611006000	2.504614000	-0.494967000
H	-4.587814000	-0.101651000	-2.248266000
H	-2.480171000	4.396792000	-1.841772000
H	-5.438440000	1.793710000	-3.602075000
H	-4.392384000	4.046710000	-3.403582000
H	-4.742779000	1.281397000	0.767553000
H	-1.753177000	-1.406147000	2.369948000
H	-5.770948000	1.466244000	3.016340000
H	-2.798464000	-1.225474000	4.611484000
H	-4.806368000	0.215242000	4.943608000

69

$Ag(Ph_3P)_2^+$_staggered Energy = -2219.608913

Ag	0.016437000	-0.007046000	-0.042241000
P	2.420754000	0.000118000	-0.019184000
P	-2.388359000	-0.008651000	-0.026450000
C	-3.101939000	1.189589000	-1.209973000
C	-2.502400000	1.322044000	-2.475460000
C	-4.225201000	1.969407000	-0.890996000
C	-3.029282000	2.211821000	-3.412942000
C	-4.743573000	2.864966000	-1.831255000
C	-4.149663000	2.985811000	-3.090632000
H	-1.621863000	0.725531000	-2.729414000
H	-4.691951000	1.882996000	0.091616000
H	-2.560384000	2.306829000	-4.393878000
H	-5.615263000	3.470124000	-1.576034000
H	-4.556317000	3.687409000	-3.821036000
C	-3.088769000	-1.642770000	-0.453370000
C	-2.487336000	-2.791058000	0.092966000
C	-4.202740000	-1.779331000	-1.296957000
C	-3.004057000	-4.056397000	-0.188877000
C	-4.710542000	-3.050418000	-1.582771000
C	-4.115664000	-4.187314000	-1.028951000
H	-1.613930000	-2.695035000	0.743806000
H	-4.670473000	-0.896057000	-1.735073000
H	-2.534464000	-4.942291000	0.242146000
H	-5.575249000	-3.149838000	-2.241236000
H	-4.514687000	-5.177569000	-1.255266000
C	-3.055926000	0.429178000	1.618991000
C	-4.193675000	-0.196427000	2.154119000
C	-2.408073000	1.437220000	2.355389000
C	-4.677261000	0.188841000	3.408177000
C	-2.900098000	1.823325000	3.603022000
C	-4.034723000	1.197819000	4.131433000
H	-4.699044000	-0.986571000	1.596057000
H	-1.516814000	1.924253000	1.950116000
H	-5.559916000	-0.303551000	3.820042000
H	-2.393597000	2.608608000	4.166856000
H	-4.414852000	1.494100000	5.110613000

C	3.101044000	-1.074126000	1.295850000	H	4.755471000	0.860225000	-1.672363000
C	4.215382000	-1.901030000	1.081420000	H	1.637565000	-2.136658000	-1.814113000
C	2.482674000	-1.057461000	2.559214000	H	5.690591000	-0.024563000	-3.793293000
C	4.707170000	-2.694396000	2.122610000	H	2.589100000	-3.022836000	-3.925629000
C	2.982795000	-1.845525000	3.596717000	H	4.616070000	-1.967493000	-4.923916000
C	4.095154000	-2.666253000	3.378750000	C	3.099891000	1.671049000	0.279321000
H	4.696507000	-1.930643000	0.102419000	C	4.231022000	1.880144000	1.085206000
H	1.607753000	-0.424983000	2.732367000	C	2.468691000	2.771345000	-0.328166000
H	5.572437000	-3.336426000	1.948662000	C	4.725305000	3.174285000	1.273140000
H	2.499329000	-1.825007000	4.574948000	C	2.971379000	4.060279000	-0.143217000
H	4.481004000	-3.288214000	4.188279000	C	4.099509000	4.263027000	0.659372000
C	3.140907000	-0.585501000	-1.594692000	H	4.722285000	1.035597000	1.571600000
C	4.280802000	0.007488000	-2.160831000	H	1.581434000	2.619257000	-0.948977000
C	2.531561000	-1.675129000	-2.242323000	H	5.602753000	3.330069000	1.903212000
C	4.806100000	-0.491654000	-3.356625000	H	2.477343000	4.908708000	-0.619874000
C	3.065561000	-2.174646000	-3.431026000	H	4.487163000	5.271977000	0.810415000
C	4.203074000	-1.581926000	-3.990185000				

Table S2. The BP86/def2-SVP optimized gas-phase geometries. For each structure, the number of atoms, the structure name and vibrational zero point energy (in Hartree) are given, followed by the Cartesian coordinates of each atom (in Å).

70

$Ag(Ph_3P)_2^+$@Ar_eclipsed Energy = -2745.258700

P	-0.386394000	-4.979069000	-6.066270000	C	2.320342000	-0.615192000	-3.206347000
Ag	1.199581000	-3.328956000	-5.277666000	C	2.983232000	-0.356890000	-1.986750000
P	2.930150000	-1.885949000	-4.390959000	C	2.490376000	0.631913000	-1.116865000
C	3.844159000	-0.974937000	-5.701970000	C	1.341339000	1.365995000	-1.457202000
C	4.126285000	-1.645560000	-6.914635000	C	0.677976000	1.110158000	-2.671542000
C	4.847637000	-0.995057000	-7.928251000	C	1.159457000	0.119817000	-3.542302000
C	5.281527000	0.330627000	-7.743675000	C	4.190246000	-2.871282000	-3.477569000
C	4.995156000	1.003611000	-6.543160000	C	5.572786000	-2.614278000	-3.605129000
C	4.279306000	0.356189000	-5.520698000	C	6.498273000	-3.379997000	-2.874084000
C	-0.302683000	-5.257455000	-7.884957000	C	6.052794000	-4.398339000	-2.013781000
C	-0.221019000	-6.554032000	-8.437958000	C	4.675835000	-4.658364000	-1.885344000
C	-0.156775000	-6.718104000	-9.833263000	C	3.746395000	-3.903758000	-2.618714000
C	-0.176429000	-5.597009000	-10.680198000	H	-0.204805000	-7.437422000	-7.781082000
C	-0.258245000	-4.303440000	-10.131919000	H	-0.376048000	-3.113524000	-8.319459000
C	-0.314725000	-4.130480000	-8.740090000	H	-0.091757000	-7.731772000	-10.258618000
C	-2.137297000	-4.562627000	-5.687177000	H	-0.273084000	-3.422580000	-10.792689000
C	-2.430537000	-3.941691000	-4.451257000	H	-0.125402000	-5.730056000	-11.772142000
C	-3.759356000	-3.641215000	-4.111887000	H	-1.615989000	-3.693471000	-3.749713000
C	-4.801178000	-3.947953000	-5.006565000	H	-2.965260000	-5.342917000	-7.552658000
C	-4.512634000	-4.557870000	-6.239875000	H	-3.982113000	-3.159693000	-3.146977000
C	-3.185044000	-4.867516000	-6.583885000	H	-5.326304000	-4.795310000	-6.942899000
C	-0.067805000	-6.615799000	-5.284471000	H	-5.842411000	-3.705633000	-4.742369000
C	-1.120599000	-7.464267000	-4.877577000	H	-2.167588000	-7.147661000	-5.004182000
C	-0.830348000	-8.715054000	-4.304571000	H	2.102022000	-6.367343000	-5.411071000
C	0.503600000	-9.126217000	-4.138428000	H	-1.654955000	-9.371749000	-3.986094000
C	1.555271000	-8.282592000	-4.541170000	H	2.601452000	-8.599975000	-4.409425000
C	1.273039000	-7.028471000	-5.105828000	H	0.725771000	-10.106659000	-3.688905000
C	1.273039000	-7.028471000	-5.105828000	H	3.883073000	-0.929111000	-1.713133000
C	1.273039000	-7.028471000	-5.105828000	H	0.633214000	-0.074670000	-4.491084000

H	3.010665000	0.827914000	-0.166318000
H	-0.223809000	1.682197000	-2.940417000
H	0.957927000	2.138526000	-0.772478000
H	4.056125000	0.889800000	-4.583618000
H	3.781526000	-2.682561000	-7.066923000
H	5.330192000	2.042599000	-6.398467000
H	5.066650000	-1.523413000	-8.869227000
H	5.841143000	0.842676000	-8.541992000
H	5.928784000	-1.818672000	-4.277843000
H	2.668743000	-4.118035000	-2.519071000
H	7.575469000	-3.176896000	-2.979229000
H	4.323432000	-5.457508000	-1.214655000
H	6.781320000	-4.995576000	-1.443474000
Ar	-0.618584000	-0.442759000	-7.104063000

70

$Ag(Ph_3P)_2^+$@He_eclipsed Energy = -2220.757302

P	-0.311819000	-5.076554000	-6.025637000
Ag	1.346154000	-3.520058000	-5.199472000
P	3.015192000	-1.985529000	-4.353651000
C	3.923135000	-1.118239000	-5.699032000
C	4.346996000	-1.872110000	-6.818110000
C	5.063840000	-1.252341000	-7.853700000
C	5.350390000	0.123881000	-7.786616000
C	4.922044000	0.878157000	-6.680685000
C	4.210567000	0.262649000	-5.635445000
C	-0.284525000	-5.231627000	-7.858820000
C	-0.470612000	-6.475033000	-8.502227000
C	-0.461965000	-6.544753000	-9.906367000
C	-0.270979000	-5.381722000	-10.672617000
C	-0.084174000	-4.141542000	-10.034898000
C	-0.084734000	-4.065224000	-8.632944000
C	-2.027037000	-4.591735000	-5.567896000
C	-2.267783000	-4.132384000	-4.251929000
C	-3.565893000	-3.770799000	-3.858589000
C	-4.628663000	-3.851666000	-4.777457000
C	-4.391375000	-4.298251000	-6.088815000
C	-3.095317000	-4.670176000	-6.487845000
C	-0.058560000	-6.775045000	-5.362708000
C	-1.135544000	-7.569271000	-4.912337000
C	-0.894055000	-8.868138000	-4.430319000
C	0.414499000	-9.380092000	-4.398449000
C	1.490146000	-8.590670000	-4.846078000
C	1.257947000	-7.290337000	-5.320912000
C	2.286807000	-0.672976000	-3.288829000
C	2.909245000	-0.253427000	-2.092591000
C	2.321991000	0.761456000	-1.316479000
C	1.119540000	1.362063000	-1.727618000
C	0.496374000	0.946003000	-2.918643000
C	1.072404000	-0.072141000	-3.694852000
C	4.294092000	-2.827588000	-3.332126000
C	5.658719000	-2.472604000	-3.410543000
C	6.600483000	-3.128189000	-2.598065000
C	6.188775000	-4.133953000	-1.706441000
C	4.830095000	-4.491192000	-1.627108000
C	3.885009000	-3.846218000	-2.440686000
H	-0.617603000	-7.390713000	-7.908584000
H	0.068562000	-3.091328000	-8.138257000
H	-0.605074000	-7.516895000	-10.403484000
H	0.069099000	-3.229221000	-10.632162000
H	-0.263105000	-5.441842000	-11.772156000
H	-1.437664000	-4.059515000	-3.529091000
H	-2.916940000	-5.017823000	-7.517270000
H	-3.747548000	-3.417958000	-2.831418000
H	-5.220681000	-4.358819000	-6.810773000
H	-5.645248000	-3.560561000	-4.470120000
H	-2.162977000	-7.173969000	-4.934463000
H	2.106442000	-6.674552000	-5.664505000
H	-1.737181000	-9.482903000	-4.078399000
H	2.516841000	-8.987927000	-4.819733000
H	0.598940000	-10.397580000	-4.019839000
H	3.850213000	-0.720548000	-1.762909000
H	0.575400000	-0.397950000	-4.623954000
H	2.809991000	1.083226000	-0.383236000
H	-0.447152000	1.412683000	-3.241984000
H	0.662793000	2.155515000	-1.115672000
H	3.876500000	0.859046000	-4.772174000
H	4.119097000	-2.949835000	-6.878865000
H	5.142445000	1.955771000	-6.627568000
H	5.395157000	-1.845094000	-8.720579000
H	5.906600000	0.610476000	-8.603020000
H	5.988036000	-1.687755000	-4.109257000
H	2.822381000	-4.136229000	-2.379978000
H	7.663779000	-2.849619000	-2.664699000
H	4.505182000	-5.281653000	-0.932724000
H	6.930154000	-4.646020000	-1.073353000
He	-1.158969000	-0.261150000	-7.067814000

71

$Ag(Ph_3P)_2^+$@N_2_eclipsed Energy = -2329.139785

P	-0.289403000	-5.158244000	-5.928234000
Ag	1.383271000	-3.622415000	-5.124330000
P	3.051685000	-2.089236000	-4.309709000
C	4.063597000	-1.372745000	-5.654250000
C	4.469040000	-2.208523000	-6.710316000
C	5.263556000	-1.703765000	-7.740823000
C	5.647834000	-0.358355000	-7.733446000
C	5.238819000	0.479477000	-6.692058000
C	4.450100000	-0.022654000	-5.652724000
C	-0.430692000	-5.143688000	-7.751972000
C	-0.597226000	-6.322754000	-8.496263000
C	-0.718875000	-6.258977000	-9.887771000

C	-0.678282000	-5.024636000	-10.542103000
C	-0.509747000	-3.847171000	-9.804898000
C	-0.379242000	-3.905364000	-8.416725000
C	-1.957378000	-4.777266000	-5.281388000
C	-2.081660000	-4.370298000	-3.940963000
C	-3.340282000	-4.100336000	-3.401619000
C	-4.483967000	-4.221686000	-4.198690000
C	-4.365564000	-4.615158000	-5.534606000
C	-3.108012000	-4.894068000	-6.078124000
C	0.067378000	-6.885850000	-5.445965000
C	-0.950126000	-7.777479000	-5.068817000
C	-0.632085000	-9.094011000	-4.722454000
C	0.695989000	-9.529039000	-4.752553000
C	1.713524000	-8.644394000	-5.126517000
C	1.402657000	-7.326673000	-5.465517000
C	2.304945000	-0.677825000	-3.418335000
C	2.893028000	-0.121949000	-2.270508000
C	2.295957000	0.975071000	-1.642153000
C	1.116588000	1.524159000	-2.153800000
C	0.525288000	0.971853000	-3.295260000
C	1.112097000	-0.128697000	-3.921325000
C	4.221151000	-2.880197000	-3.146868000
C	5.603353000	-2.639402000	-3.202396000
C	6.457501000	-3.254750000	-2.282038000
C	5.940437000	-4.106802000	-1.302516000
C	4.563797000	-4.351978000	-1.244566000
C	3.707527000	-3.748243000	-2.166224000
H	-0.626933000	-7.290117000	-7.991918000
H	-0.238277000	-2.982908000	-7.847153000
H	-0.845485000	-7.179286000	-10.460605000
H	-0.471861000	-2.882011000	-10.312817000
H	-0.771819000	-4.979152000	-11.628506000
H	-1.190939000	-4.265284000	-3.315620000
H	-3.023510000	-5.197081000	-7.123186000
H	-3.427931000	-3.787200000	-2.359820000
H	-5.255289000	-4.705748000	-6.160217000
H	-5.467312000	-4.003270000	-3.778730000
H	-1.988672000	-7.443509000	-5.039000000
H	2.202825000	-6.636442000	-5.746352000
H	-1.427185000	-9.780815000	-4.426982000
H	2.752115000	-8.979035000	-5.146061000
H	0.940002000	-10.556956000	-4.478833000
H	3.812468000	-0.547133000	-1.864148000
H	0.640889000	-0.563349000	-4.807126000
H	2.756128000	1.400917000	-0.748793000
H	-0.398704000	1.394126000	-3.693958000
H	0.653722000	2.379941000	-1.659347000
H	4.131715000	0.638017000	-4.844574000
H	4.163555000	-3.258102000	-6.726774000
H	5.533487000	1.530341000	-6.686067000
H	5.576298000	-2.359461000	-8.555262000
H	6.262201000	0.037775000	-8.543822000
H	6.014177000	-1.976119000	-3.965278000
H	2.634112000	-3.950602000	-2.120732000
H	7.531094000	-3.065006000	-2.332523000
H	4.157247000	-5.020916000	-0.484071000
H	6.610165000	-4.585665000	-0.586119000
N	-1.036654000	1.846697000	-9.311249000
N	-1.284030000	2.794586000	-9.818292000

70

$Ag(Ph_3P)_2^+$@Ne_eclipsed Energy = -2346.662030

P	-0.350924000	-5.024259000	-6.050931000
Ag	1.267497000	-3.417762000	-5.241851000
P	2.967433000	-1.932974000	-4.369385000
C	3.872403000	-1.038121000	-5.697746000
C	4.203839000	-1.743854000	-6.877551000
C	4.919177000	-1.105110000	-7.902796000
C	5.297379000	0.243063000	-7.763037000
C	4.961355000	0.950453000	-6.595747000
C	4.251200000	0.315389000	-5.561581000
C	-0.293687000	-5.247392000	-7.877689000
C	-0.295796000	-6.527594000	-8.473035000
C	-0.253712000	-6.648897000	-9.873471000
C	-0.212778000	-5.501183000	-10.683429000
C	-0.210393000	-4.223723000	-10.092950000
C	-0.243933000	-4.093984000	-8.695720000
C	-2.084361000	-4.565224000	-5.638035000
C	-2.351269000	-4.046043000	-4.349851000
C	-3.664037000	-3.707985000	-3.985378000
C	-4.715335000	-3.873317000	-4.906177000
C	-4.452244000	-4.380629000	-6.190354000
C	-3.141001000	-4.729026000	-6.560084000
C	-0.071206000	-6.689440000	-5.318738000
C	-1.144608000	-7.529056000	-4.948289000
C	-0.884473000	-8.803715000	-4.415012000
C	0.439659000	-9.247244000	-4.252759000
C	1.511487000	-8.412536000	-4.619233000
C	1.259455000	-7.134917000	-5.144083000
C	2.306063000	-0.642373000	-3.235094000
C	2.941361000	-0.330405000	-2.013483000
C	2.407820000	0.669763000	-1.181403000
C	1.245698000	1.362298000	-1.561842000
C	0.609838000	1.053528000	-2.778693000
C	1.131787000	0.051200000	-3.611520000
C	4.240688000	-2.856034000	-3.411473000
C	5.615147000	-2.547711000	-3.511056000
C	6.551425000	-3.266288000	-2.746828000
C	6.124648000	-4.288420000	-1.881393000
C	4.756047000	-4.599484000	-1.780946000
C	3.816193000	-3.891997000	-2.547332000
H	-0.327417000	-7.431285000	-7.844976000

H	-0.238120000	-3.090699000	-8.240539000
H	-0.253646000	-7.649936000	-10.332347000
H	-0.176538000	-3.322113000	-10.724346000
H	-0.179316000	-5.601085000	-11.779575000
H	-1.528938000	-3.908409000	-3.627359000
H	-2.940972000	-5.124959000	-7.567881000
H	-3.866682000	-3.307708000	-2.979752000
H	-5.273125000	-4.507776000	-6.913311000
H	-5.743702000	-3.600852000	-4.621769000
H	-2.183975000	-7.186650000	-5.071488000
H	2.103742000	-6.480519000	-5.420551000
H	-1.724683000	-9.453718000	-4.124836000
H	2.549833000	-8.755511000	-4.489674000
H	0.638365000	-10.246313000	-3.834349000
H	3.851507000	-0.869444000	-1.708572000
H	0.626742000	-0.187348000	-4.561276000
H	2.906528000	0.907546000	-0.228830000
H	-0.302063000	1.592803000	-3.079163000
H	0.830440000	2.143909000	-0.906648000
H	3.988324000	0.875848000	-4.650827000
H	3.902814000	-2.798935000	-6.993925000
H	5.252908000	2.006713000	-6.486301000
H	5.177297000	-1.660492000	-8.817950000
H	5.852413000	0.745329000	-8.570708000
H	5.956734000	-1.749531000	-4.188311000
H	2.745491000	-4.146540000	-2.470558000
H	7.622321000	-3.023690000	-2.830296000
H	4.418767000	-5.402216000	-1.106789000
H	6.861638000	-4.849130000	-1.285470000
Ne	-0.255650000	-1.034405000	-6.801221000

70

$Ag(Ph_3P)_2^+$@Ar_staggered Energy = -2745.258301

Ag	-0.217777000	0.320051000	-0.761353000
P	2.089657000	0.764297000	-1.348833000
P	-2.569289000	0.073123000	-0.237343000
C	-3.545061000	1.477816000	-0.921723000
C	-3.338135000	1.837663000	-2.274272000
C	-4.483224000	2.190887000	-0.144713000
C	-4.071894000	2.890050000	-2.843505000
C	-5.208149000	3.250358000	-0.719684000
C	-5.006147000	3.599561000	-2.065708000
H	-2.606767000	1.286259000	-2.889338000
H	-4.648619000	1.922174000	0.910116000
H	-3.911569000	3.160401000	-3.898958000
H	-5.937627000	3.804164000	-0.108262000
H	-5.576936000	4.429051000	-2.511531000
C	-3.351683000	-1.452650000	-0.904822000
C	-2.612452000	-2.657689000	-0.891984000
C	-4.671584000	-1.445984000	-1.408439000
C	-3.193741000	-3.844503000	-1.366645000
C	-5.243882000	-2.636904000	-1.888219000
C	-4.508563000	-3.834926000	-1.866767000
H	-1.580286000	-2.671350000	-0.505973000
H	-5.251334000	-0.510147000	-1.430957000
H	-2.614414000	-4.780876000	-1.352062000
H	-6.272163000	-2.626240000	-2.282148000
H	-4.960282000	-4.765042000	-2.245612000
C	-2.876163000	0.067903000	1.577310000
C	-3.819141000	-0.797372000	2.173235000
C	-2.141921000	0.967584000	2.384905000
C	-4.027084000	-0.755036000	3.563366000
C	-2.361557000	1.010746000	3.770758000
C	-3.302922000	0.147504000	4.361357000
H	-4.388779000	-1.507049000	1.553423000
H	-1.398042000	1.641571000	1.926844000
H	-4.761707000	-1.433698000	4.024209000
H	-1.791239000	1.717266000	4.393827000
H	-3.469070000	0.176319000	5.449578000
C	3.300317000	0.256154000	-0.060092000
C	4.544789000	-0.321239000	-0.395112000
C	2.973993000	0.478139000	1.297449000
C	5.453056000	-0.665958000	0.621484000
C	3.888475000	0.137938000	2.306772000
C	5.128403000	-0.435606000	1.969641000
H	4.804743000	-0.505589000	-1.449179000
H	1.999566000	0.919401000	1.566986000
H	6.421501000	-1.117638000	0.355409000
H	3.629336000	0.314627000	3.362332000
H	5.842317000	-0.708492000	2.762425000
C	2.588844000	-0.102924000	-2.894412000
C	3.244285000	0.566349000	-3.950348000
C	2.289487000	-1.480538000	-3.015968000
C	3.600227000	-0.139976000	-5.113315000
C	2.654628000	-2.179712000	-4.176891000
C	3.307993000	-1.509644000	-5.228066000
H	3.476132000	1.639473000	-3.868134000
H	1.778676000	-2.011053000	-2.195433000
H	4.110385000	0.387353000	-5.934504000
H	2.423078000	-3.252750000	-4.264104000
H	3.587334000	-2.058162000	-6.141143000
C	2.382370000	2.557911000	-1.641088000
C	3.593385000	3.182272000	-1.268373000
C	1.367147000	3.318356000	-2.265911000
C	3.784681000	4.550755000	-1.526906000
C	1.567869000	4.683280000	-2.527446000
C	2.776381000	5.300850000	-2.156972000
H	4.386508000	2.602710000	-0.770815000
H	0.413093000	2.842038000	-2.548450000
H	4.729457000	5.033050000	-1.231223000
H	0.773535000	5.269286000	-3.015428000
H	2.929851000	6.373160000	-2.355101000

Ar	1.021385000	-2.928887000	0.722794000

70

$Ag(Ph_3P)_2^+$@He_staggered Energy = -2220.75766

Ag	-0.242849000	0.564787000	-0.827586000
P	2.079262000	0.897468000	-1.416428000
P	-2.565120000	0.233103000	-0.238920000
C	-3.710124000	1.212790000	-1.295849000
C	-3.449636000	1.284653000	-2.684201000
C	-4.836082000	1.875100000	-0.759902000
C	-4.314556000	2.000565000	-3.526881000
C	-5.693660000	2.596544000	-1.609203000
C	-5.436141000	2.659081000	-2.989602000
H	-2.568709000	0.775392000	-3.110678000
H	-5.042449000	1.831064000	0.320723000
H	-4.108578000	2.049938000	-4.607491000
H	-6.569240000	3.113445000	-1.186296000
H	-6.109782000	3.226750000	-3.650365000
C	-3.083170000	-1.524522000	-0.408606000
C	-2.187027000	-2.534854000	0.011667000
C	-4.343716000	-1.882749000	-0.934902000
C	-2.554756000	-3.886583000	-0.081239000
C	-4.702083000	-3.238926000	-1.032056000
C	-3.812143000	-4.239636000	-0.605008000
H	-1.196832000	-2.264669000	0.416402000
H	-5.045292000	-1.104843000	-1.274226000
H	-1.854072000	-4.668205000	0.250467000
H	-5.685104000	-3.513112000	-1.445757000
H	-4.096838000	-5.300418000	-0.684625000
C	-2.925452000	0.717555000	1.499460000
C	-3.752678000	-0.063346000	2.335665000
C	-2.359430000	1.915490000	1.994823000
C	-4.013998000	0.357176000	3.651814000
C	-2.630690000	2.332449000	3.307538000
C	-3.456993000	1.552625000	4.137862000
H	-4.190583000	-1.001972000	1.962118000
H	-1.707028000	2.528998000	1.350503000
H	-4.658468000	-0.256289000	4.300663000
H	-2.190157000	3.267985000	3.686095000
H	-3.663654000	1.877131000	5.169665000
C	3.225366000	-0.079746000	-0.358421000
C	4.352514000	-0.740668000	-0.893590000
C	2.964549000	-0.151097000	1.029893000
C	5.210936000	-1.460238000	-0.043558000
C	3.830319000	-0.865119000	1.873309000
C	4.953074000	-1.522267000	1.336805000
H	4.559143000	-0.696994000	-1.974181000
H	2.082672000	0.357047000	1.455731000
H	6.087441000	-1.976066000	-0.465856000
H	3.624075000	-0.914105000	2.953886000
H	5.627377000	-2.088469000	1.998150000
C	2.440227000	0.411567000	-3.154262000
C	3.267274000	1.192050000	-3.991044000
C	1.874911000	-0.787137000	-3.648571000
C	3.529131000	0.770347000	-5.306707000
C	2.146695000	-1.205258000	-4.960810000
C	2.972828000	-0.425859000	-5.791700000
H	3.704639000	2.131268000	-3.618351000
H	1.222634000	-1.400311000	-3.003806000
H	4.173454000	1.383484000	-5.956012000
H	1.706698000	-2.141375000	-5.338551000
H	3.179893000	-0.751282000	-6.823132000
C	2.595394000	2.655900000	-1.248666000
C	3.855287000	3.016250000	-0.722266000
C	1.698160000	3.664685000	-1.670323000
C	4.211995000	4.372965000	-0.626335000
C	2.064370000	5.016879000	-1.578533000
C	3.321037000	5.372226000	-1.054665000
H	4.557689000	2.239555000	-0.381870000
H	0.708465000	3.392887000	-2.075197000
H	5.194530000	4.648741000	-0.212542000
H	1.362472000	5.797375000	-1.911325000
H	3.604355000	6.433439000	-0.975976000
He	-0.158873000	-6.904786000	1.094688000

70

$Ag(Ph_3P)_2^+$@Ne_staggered Energy = -2346.66127

Ag	-0.220938000	0.443603000	-0.736718000
P	2.085008000	0.805703000	-1.373671000
P	-2.562144000	0.137005000	-0.207488000
C	-3.635019000	1.334476000	-1.102613000
C	-3.314546000	1.661354000	-2.440625000
C	-4.767629000	1.916966000	-0.492595000
C	-4.126502000	2.550580000	-3.162764000
C	-5.571313000	2.813081000	-1.219077000
C	-5.254378000	3.128836000	-2.551743000
H	-2.427041000	1.217057000	-2.922571000
H	-5.020528000	1.675011000	0.551473000
H	-3.874001000	2.798141000	-4.205646000
H	-6.451466000	3.267177000	-0.737644000
H	-5.886271000	3.832074000	-3.116393000
C	-3.176980000	-1.541832000	-0.647555000
C	-2.386357000	-2.659677000	-0.290226000
C	-4.399152000	-1.737067000	-1.326729000
C	-2.823654000	-3.957358000	-0.598685000
C	-4.825749000	-3.040319000	-1.639181000
C	-4.042340000	-4.149014000	-1.275776000
H	-1.430402000	-2.515113000	0.237745000
H	-5.018251000	-0.873662000	-1.615646000
H	-2.206609000	-4.823722000	-0.313388000
H	-5.778781000	-3.187299000	-2.170964000
H	-4.380375000	-5.167387000	-1.523381000

C	-2.920007000	0.365877000	1.582806000
C	-3.830176000	-0.462914000	2.274725000
C	-2.267396000	1.416252000	2.268817000
C	-4.086330000	-0.235214000	3.638528000
C	-2.532847000	1.641369000	3.628799000
C	-3.441550000	0.814706000	4.315128000
H	-4.336120000	-1.289156000	1.751189000
H	-1.550360000	2.063688000	1.735917000
H	-4.795339000	-0.885292000	4.174606000
H	-2.023964000	2.462683000	4.157109000
H	-3.644122000	0.987833000	5.383603000
C	3.290140000	-0.000181000	-0.239770000
C	4.355729000	-0.791951000	-0.719781000
C	3.128330000	0.187487000	1.152993000
C	5.253600000	-1.382038000	0.187881000
C	4.034110000	-0.396828000	2.051786000
C	5.096688000	-1.184045000	1.570160000
H	4.486382000	-0.950858000	-1.801415000
H	2.293960000	0.797950000	1.537100000
H	6.082505000	-1.999711000	-0.191646000
H	3.906670000	-0.242323000	3.134644000
H	5.802490000	-1.647616000	2.276964000
C	2.428891000	0.147061000	-3.056788000
C	3.317680000	0.796649000	-3.941671000
C	1.789795000	-1.048442000	-3.458858000
C	3.565473000	0.248802000	-5.212319000
C	2.046631000	-1.593249000	-4.727391000
C	2.933424000	-0.943974000	-5.605580000
H	3.812729000	1.733410000	-3.641736000
H	1.087093000	-1.556661000	-2.776645000
H	4.256856000	0.760561000	-5.899886000
H	1.546556000	-2.525140000	-5.034006000
H	3.128676000	-1.367471000	-6.603175000
C	2.534558000	2.589984000	-1.415735000
C	3.795455000	3.052416000	-0.978928000
C	1.587595000	3.509990000	-1.922006000
C	4.103366000	4.422270000	-1.055453000
C	1.904322000	4.875331000	-2.000770000
C	3.162066000	5.332753000	-1.566194000
H	4.536102000	2.344774000	-0.574890000
H	0.597901000	3.157171000	-2.258441000
H	5.086982000	4.778630000	-0.711648000
H	1.163241000	5.586879000	-2.397089000
H	3.406834000	6.404970000	-1.621666000
Ne	0.494321000	-1.805795000	1.515371000

71

$Ag(Ph_3P)_2^+$@N2_staggered Energy =-2329.140161

Ag	-0.241744000	0.574306000	-0.946423000
P	2.055148000	0.933807000	-1.571308000
P	-2.546049000	0.231265000	-0.339950000
C	-3.669256000	1.266488000	-1.348706000
C	-3.445423000	1.342099000	-2.735570000
C	-4.735364000	1.981134000	-0.780147000
C	-4.287190000	2.109164000	-3.542297000
C	-5.570291000	2.754752000	-1.592411000
C	-5.349805000	2.818243000	-2.970914000
H	-2.614007000	0.794959000	-3.188245000
H	-4.912391000	1.936742000	0.295528000
H	-4.109335000	2.158693000	-4.617953000
H	-6.396693000	3.308679000	-1.143642000
H	-6.003184000	3.424060000	-3.601105000
C	-3.086439000	-1.499060000	-0.580477000
C	-2.212990000	-2.533449000	-0.197650000
C	-4.343110000	-1.818300000	-1.119566000
C	-2.598527000	-3.867013000	-0.339448000
C	-4.719996000	-3.156775000	-1.267774000
C	-3.852093000	-4.179998000	-0.877210000
H	-1.229928000	-2.295586000	0.217490000
H	-5.025347000	-1.025176000	-1.429777000
H	-1.917364000	-4.663957000	-0.036368000
H	-5.697095000	-3.397852000	-1.690067000
H	-4.149514000	-5.223448000	-0.994829000
C	-2.887646000	0.645142000	1.407854000
C	-3.774901000	-0.110568000	2.190832000
C	-2.247935000	1.764714000	1.970250000
C	-4.022256000	0.255886000	3.517182000
C	-2.505546000	2.130919000	3.292129000
C	-3.392044000	1.375371000	4.067664000
H	-4.268385000	-0.987695000	1.769035000
H	-1.548733000	2.354897000	1.371644000
H	-4.710629000	-0.337990000	4.120995000
H	-2.007815000	3.002693000	3.720330000
H	-3.586738000	1.657409000	5.103811000
C	3.207060000	-0.048892000	-0.543534000
C	4.344818000	-0.667910000	-1.085568000
C	2.943663000	-0.165979000	0.833139000
C	5.209656000	-1.388845000	-0.256590000
C	3.815779000	-0.878334000	1.657530000
C	4.948886000	-1.492670000	1.112507000
H	4.552496000	-0.592110000	-2.154111000
H	2.054593000	0.303686000	1.262928000
H	6.090096000	-1.871075000	-0.684901000
H	3.606974000	-0.960815000	2.725521000
H	5.625938000	-2.057016000	1.756073000
C	2.397588000	0.477888000	-3.308332000
C	3.222330000	1.259144000	-4.133765000
C	1.825074000	-0.701853000	-3.817055000
C	3.475268000	0.857861000	-5.449006000
C	2.088071000	-1.101656000	-5.128057000
C	2.912655000	-0.321089000	-5.945993000
H	3.661837000	2.182640000	-3.753351000

H	1.175150000	-1.312544000	-3.184546000
H	4.115282000	1.470715000	-6.086152000
H	1.643217000	-2.020285000	-5.514471000
H	3.112448000	-0.630896000	-6.973197000
C	2.558532000	2.681814000	-1.380942000
C	3.811996000	3.042394000	-0.860450000
C	1.656913000	3.686980000	-1.775213000
C	4.158180000	4.392016000	-0.743508000
C	2.011724000	5.032262000	-1.664515000
C	3.262428000	5.386291000	-1.146335000
H	4.516270000	2.272695000	-0.540295000
H	0.674644000	3.417440000	-2.172660000
H	5.132858000	4.664868000	-0.335209000
H	1.307849000	5.805861000	-1.976277000
H	3.535764000	6.438635000	-1.052064000
N	0.410070000	-5.573693000	5.602753000
N	0.132358000	-5.018625000	4.690889000